Ozone_cci

Comprehensive Error Characterization Report (CECR) Version 2

Reference: Ozone_cci_KIT_CECR_02_01_02

Date of issue: 22/12/2016

Distributed to: Ozone_cci Consortium

WP Manager: P. Braesicke
WP Manager Organization: KIT

Other partners:
EOST: DLR-IMF, KNMI, IUP, LATMOS, ULB, FMI, University of Saskatchewan, University of Toronto, Chalmers University of Technology, Meteo-Swiss, RAL, LATMOS, IULB
CRG: DLR-PA

This work is supported by the European Space Agency

DOCUMENT PROPERTIES

Title	CECR version 2
Reference	Ozone_cci_KIT_CECR_02_01_02
Issue	01
Revision	02
Status	
Date of issue	22/12/2016
Document type	Deliverable

	FUNCTION	NAME	DATE
Lead author	EOST-2	Alexandra Laeng,	20/05/2016
Contributing authors	EOST-2 VALT Leader VALT EOST-1	Thomas von Clarmann Gabriele Stiller Viktoria Sofieva Nabiz Rahpoe Doug Deggenstein Kaley Walker Donald Murtagh Jean-Christopher Lambert Tijl Verhoelst Christophe Lerot Cathy Clerbeaux Anne Boyard Klaus-Peter Heue Jacob van Peet Richard Siddans Rosa Astoreca Juliette Hadji-Lazaro	
REVIEWED BY	ESA Technical Officer	Claus Zehner	
ISSUED BY	EOST-2	Alexandra Laeng	20/05/2016

DOCUMENT CHANGE RECORD

Issue	**Revision**	**Date**	**Modified items**	**Observations**
00	00	25/03/2016		Creation of document
00	01	26/03/2016	Chapter about OSSE added	
00	01	22/12/2016	OMPS-LP USask 2D errors description is added. Description of CCD errors is updated.	

Contents

Executive summary

The Comprehensive Error Characterisation Report version 0 (CECRv0) is a deliverable of the ESA Ozone_cci project (http://www.esa-ozone-cci.org/). The Ozone_cci project is one of twelve projects of ESA's Climate Change Initiative (CCI). The Ozone_cci project is delivering the Essential Climate Variable (ECV) Ozone in line with the "Systematic observation requirements for satellite-based products for climate" as defined by GCOS (Global Climate Observing System) in (GCOS-107, 2006): "Product A.7: Profile and total column of ozone".

The present document provides the error analysis: error characterization of Level 2 and Level 3 products, partly based on information already given in ATBD, and validation of uncertainty estimates of Level 2 products.. All the products are available at http://www.esa-ozone-cci.org/?q=node/160

1. Introduction

The comprehensive characterization of the uncertainties provided with the datasets is one of the main objectives of the ESA Climate Change Initiative. During the Phase 1 of Ozone_cci project (September 2010 – August 2013), the ATBD of Ozone_cci Project englobed the characterisation of error budget of Level 1 and 2 products, together with description of the algorithms. Some teams of the consortium have performed the geophysical validation of their error estimates. The purpose of this document is to collect in one place the characterization and geophysical validation of uncertainty estimates of all individual Level 2 datasets participating in the project and provide characterizations of errors of all Level 3 ECV generated within the project.

2. Applicable documents

Ozone_cci ATBD
Ozone_cci PVASR
ESA CCI Project Guidelines

3. Summary of terminology

During Phase 1, a special effort was done by the consortium to establish a common terminology in uncertainties characterization.

The ***"precision"*** of an instrument/retrieval characterizes is its random (in the time domain) error. It is the debiased root mean square deviation of the measured values from the true values. The precision can also be seen as scatter of multiple measurements of the same quantity. The difference between the measured and the true state can still be large, because there still can be a large systematic error component unaccounted by the precision.

The ***"bias"*** of an instrument/retrieval characterizes its systematic (in the time domain) error. It is the mean difference of the measured values from the true values.

The ***"total error"*** of an instrument/retrieval characterizes the estimated total difference between the measured and the true value. In parts of the literature the expected total error is called "accuracy" but we suggest not using this particular term because its use in the literature is ambiguous.

Some teams use ***"smoothing error"*** concept, despite the fact that smoothing error does not follow Gaussian error propagation. Pros and cons of smoothing error are discussed in details in (von Clarmann 2014).

4. Uncertainties of Level 2 data

Table 1 summarizes the status of publications on error budget evaluation and uncertainties validation of Level 2 ECV's generated within Ozone_cci.

Sensor	Product	Algorithm	Error budget publication	Uncertainty validation publication
GOME GOME-2 SCIAMACHY OMI	Total column	GODFIT3	(Lerot et al. 2014)	(Verhoelst et al. 2015)
GOME GOME-2 SCIAMACHY OMI	Nadir profile	RAL	(Siddans 2003) (Miles et al. 2015)	(Laeng et al. 2016)
IASI	Nadir profile	FORLI	(Hurtmans et al. 2012), (Dufour et al. 2012)	• (Laeng et al. 2016)
• GOMOS	• Limb profile	• IPF V.6	(Tamminen et al. 2010)	(Sofieva et al. 2014)
MIPAS	Limb profile	IMK Scientific	(Steck et al. 2007)	(Laeng et al. 2015)
SCIAMACHY	Limb profile	IUP Scientific	(Rahpoe et al. 2013)	(Laeng et al. 2016)
ACE-FTS	Limb profile		(Dupuy et al. 2008)	(Laeng et al. 2016)
OSIRIS	Limb profile		(Bourassa et al. 2012)	(Bourassa et al. 2012)
SMR	Limb profile	CTSO	(Urban et al. 2005)	(Laeng et al. 2016)
SCIAMACHY	Tropospheric column	Limb Nadir Matching	(Ebojie et al. 2014)	
GOME-2	Tropospheric column	CCD	(Valks et al. 2014)	
IASI	Tropospheric column		(Dufour et al. 2012)	

Table 1: summary of error budget characterization and precision validation publications of Ozone_cci consortium.

While all products published their error characterizations, very few published geophysical validation of their uncertainties estimates.

4.1. Characterization of uncertainty estimates

This section, partly based on ATBD, recompiles error analysis of Level 2 processors. Error budgets of processors are presented in a synthetic ways (either summary tables or summary figures).

4.1.1. Ozone total column

4.1.1.1. GODFIT

Within the Ozone_cci project, the baseline algorithm for total ozone retrieval from backscatter UV sensors is the GOME-type direct-fitting (GODFIT) algorithm. Dominant error sources are:

- Ozone cross-sections uncertainties,
- Level-1 calibration limitations,
- Interferences with other species, including aerosols,
- Cloud contamination,
- A priori O3 profile shape, especially at large solar zenith angles.

Figure 1 shows that the mean total ozone error due to the profile shape is less than 0.5 % at low SZAs and is as large as 4% at extreme SZA for clear sky pixels. In the case of cloud contamination, the error increases, especially at low SZA.

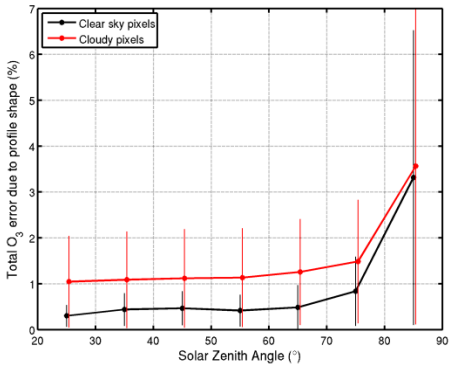

Figure 1: mean total ozone error due to a priori O3 profile shape, as a function of the SZA for clear sky and cloudy pixels. Error bars represent the standard deviation of the errors.

Figure 2 illustrates the total ozone errors due to the neglect of aerosols in the forward model for different types of atmospheric aerosols content. These errors are generally within 1%. In particular, it is shown that the fit of the surface albedo leads to a minimization of the errors, which would be much larger without that procedure (up to 4%) in case of heavily polluted conditions. For a scenario with a strong injection of stratospheric aerosols due to a major volcanic eruption such as Pinatubo, the total errors may reach 10% (right panel).

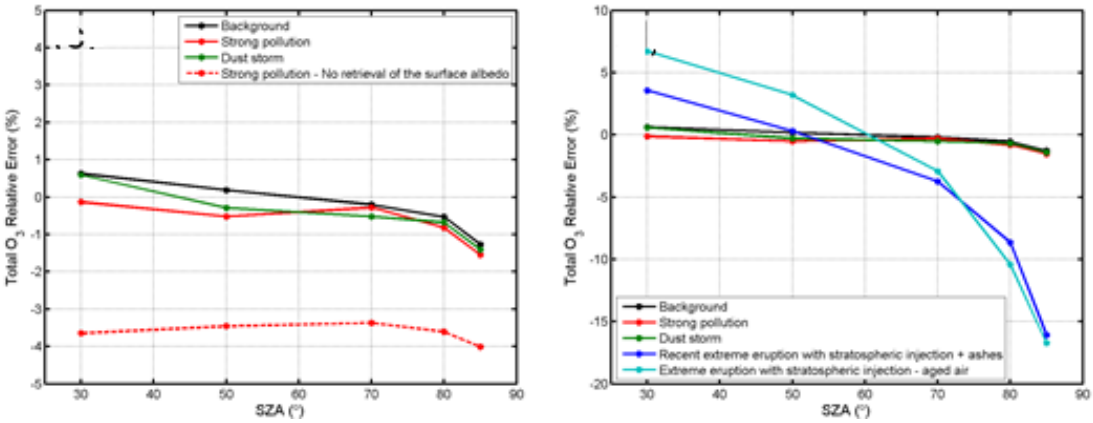

Figure 2: Left: total ozone error (%) due to neglect of aerosols in the retrieval scheme, polluted and dust storm scenarios. Right: same for strong volcanic eruption scenarios.

Table 2 summarizes current assessment of the main contributions to the global error budget on total ozone retrieval by GODFIT. Total errors are computed assuming all contributions are mutually uncorrelated.

Error source	Per cent error	
	SZA < 80°	SZA > 80°
Instrument signal-to-noise	< 0.5	< 2
Soft calibration: Absolute recalibration + structures removal	< 1.5	< 1.5
O_3 absorption cross-sections and its atmospheric temperature	< 2.5	< 2.5
Interferences with other species (except in case of volcanic eruption)	< 1.5	< 1
Aerosols (except in case of volcanic eruption)	< 1	< 1.5
Instrument spectral stability (wavelength registration)	< 0.5	< 0.5
Solar I_0-effect	< 0.2	< 0.2
Ring effect (Rotational Raman Scattering)	< 0.1	< 0.5
O_3 profile shape	< 1	< 4
Cloud fraction	< 0.5	< 0.5
Cloud top height	< 1.5	< 1.5
Total random error (including cloud fields)	**< 1.7**	**< 2.6**
Total systematic error	**< 3.6**	**< 5.3**

Table 2 : Estimation of the error sources of the direct-fitting total ozone retrievals (single pixel retrieval). Blue fields indicate random errors (precision) associated with instrument signal-to-noise and which can be derived easily by the propagation of radiance and irradiance statistical errors provided in the level-1 products through the inversion algorithm, and red fields systematic errors. The errors due to the cloud parameters (orange) are random or systematic depending on the time scale.

4.1.2. Nadir ozone vertical profile

After completion of the Round-Robin intercomparison exercise in Phase 1 of the project, RAL (Rutherford Appleton Laboratory) ozone profile retrieval scheme for nadir looking

instruments was selected as the CCI baseline algorithm, and contributed to the generation of the first version of Ozone_cci CRDP. Additionally, in Phase 2, the UV/VIS GOME-type nadir sensors (GOME, GOME-2, SCIAMACHY, OMI) are completed by IR sensors IASI, whose algorithm is enhanced and adapted for consistency with UV nadir sensors. This section reports error analysis of corresponding algorithms, RAL scheme and FORLI.

4.1.2.1. RAL

Analysis of error budget of RAL scheme, reported in (Siddans 2003), is based on performing retrieval simulations for a set of basic geo-physical scenario which had been defined for the GOME-2 Error Study (Kerridge et al. 2002). Figure 3 shows retrieval precision and base-line mapped errors for GOME-1 and the April 55ºN scenario from (Siddans 2003). Dashed and solid lines refer to the 80% and 5% surface albedo cases respectively. Colours distinguish results for the 3 across-track ground pixels in B1 (the legend shows the pixel mean off-nadir angle in degrees; positive angle are East of nadir). Dotted lines in each panel other than the top left show (for comparison) the precision where the scale permits. The black dash-dot curve is the a priori error input to the B1 retrieval. Retrieval precision and a priori are also plotted as negative values for comparison with negative mapped errors.

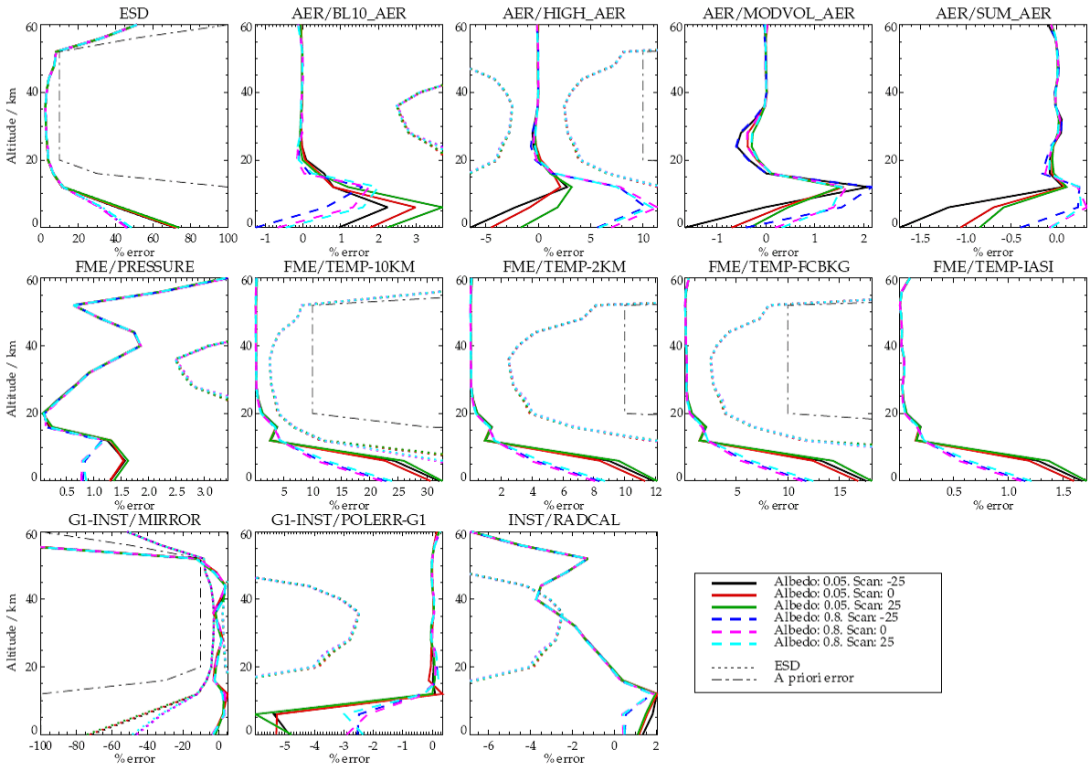

Figure 3: retrieval precision and base-line mapped errors for GOME-1 and the April 55ºN scenario.

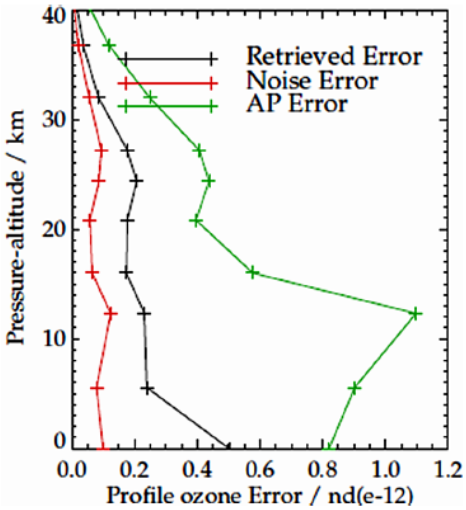

Figure 4: error assessment for ozone profile for a GOME-2 nadir pixel at 45ºN on 25 August 2008.

(Miles et al. 2015) assesses the performance of the RAL ozone profile retrieval scheme for the GOME-2 with a focus on tropospheric ozone. The retrieval precision, as given by the square roots of diagonals of the solution error covariance matrix is generally in the few percent range in the stratosphere increasing to a few tens of percent in the lowest retrieval levels. An example is presented in Figure 4 for a mid-latitude profile in Northern Hemisphere summer. In this case, the retrieval precision on retrieval levels is typically much smaller than the a priori error throughout the profile. The retrieval noise error is around a factor of 2 smaller than the retrieval precision.

Figure 5 shows an example of how the retrieval precision varies for a typical orbit cross-section; the uncertainty values are higher at lower altitudes in tropical and polar conditions.

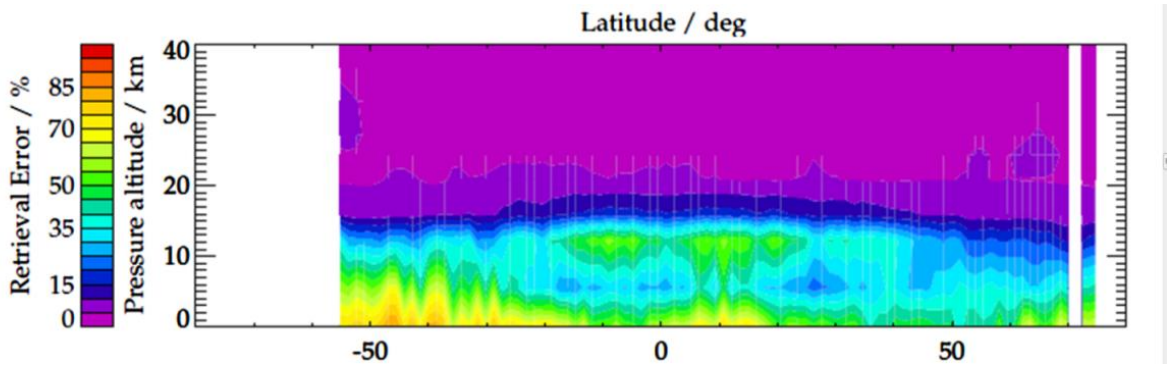

Figure 5: relative retrieval error of ozone product from GOME-2 retrieved with RAL scheme.

4.1.2.1. IASI FORLI

Fast Optimal Retrievals on Layers for IASI (FORLI) algorithm. Main contributions to the total error come from the limited vertical sensitivity (smoothing error), from the measurement noise and from uncertainties on fitted water vapour column, or fixed parameters such as surface emissivity and temperature profiles.

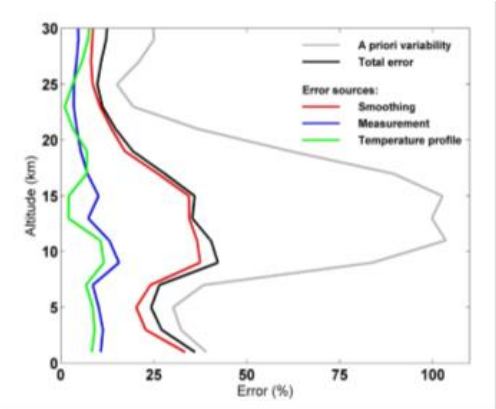

Figure 6: error budget analysis for IASI FORLI ozone retrievals.

In the routine processing of the error matrix, the error introduced by uncertainties on the fixed parameters is not taken into account. For ozone, the error is larger in the tropics (above 30%) due to the increase in humidity and also above cold surfaces, possibly due to a misrepresentation of the emissivity in the polar regions (Hurtmans et al. 2012, Wespes et al. 2009).

Altitude range	0-40 km
Vertical resolution	~7 km troposphere, ~15 km stratosphere
Random errors : Measurement error Smoothing error	 <10% over all the profile 10-35% troposphere, 5-30% MLS, <10% upper stratosphere
Systematic errors : Uncertainty in cross-sections Temperature uncertainty	 ~4% <10% over all the profile

Table 3 : IASI ozone profiles characteristics and error budget.

There is no bias due to instrument aging: when comparing IASI/MetOpA et IASI/MetOpB, the radiance signals are similar (see Figure 7)Figure 7: IASI O_3 retrieval (0 - 6 km) for IASI-A and -B, in different parts of the globe..

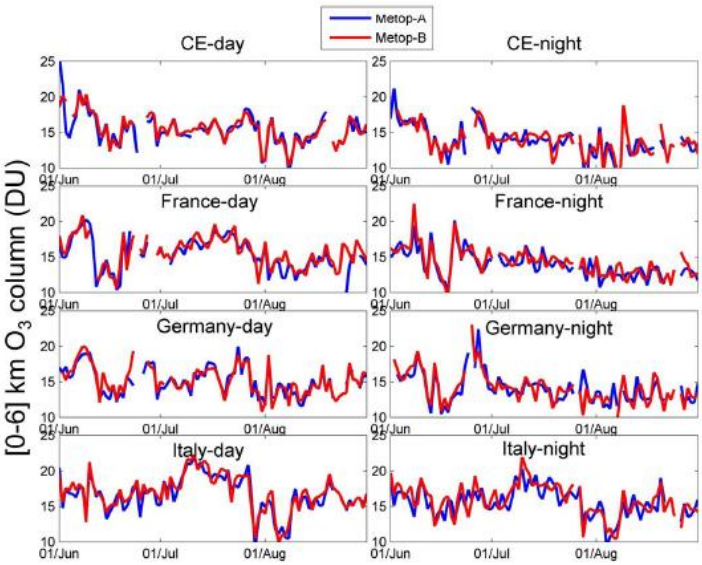

Figure 7: IASI O_3 retrieval (0 - 6 km) for IASI-A and -B, in different parts of the globe.

4.1.3. Limb ozone vertical profile

4.1.3.1. MIPAS IMK Scientific

Figure 8 shows the MIPAS ozone error budget for full spectral resolution (FR) period of MIPAS instrument (2002-2004) averaged over one orbit. Below 15 km the percentage errors are rapidly increasing to values in the order of 25% for polar and midlatitude conditions or more than 50% for tropical conditions, where the vmr is small. The error in vmr remains below 0.5 ppmv. The estimated random error is dominated by the instrumental noise above 14 km. Below 14 km, the error due to uncertain water vapor concentration becomes dominant because water vapor increase exponentially with decreasing altitude, these strong water vapor lines are slightly interfering with ozone lines leading to a dependence of the retrieved ozone on the pre-retrieved water vapor amount.

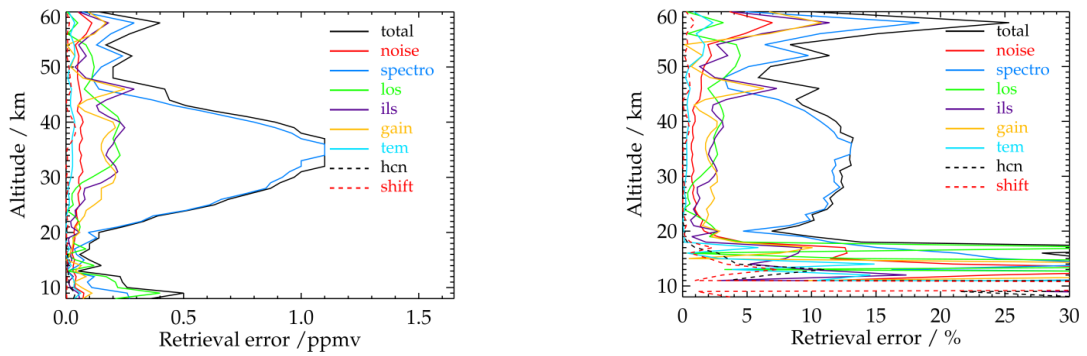

Figure 8: Estimated ozone error budget of MIPAS for a typical FR mid-latitude retrieval (night and day). Left: absolute, right: percentage errors.

The error is dominated by uncertainties in spectroscopic data (dark blue). The altitude-dependence of errors due to spectroscopic data is due to the fact that the microwindows used in the retrieval are varying with altitude. Errors caused by uncertainties in the ILS (instrumental line shape) are in the order of 1 to 4% and thus nearly negligible compared to spectroscopic uncertainties.

Figure 9 reports a similar error budget analysis of MIPAS IMK ozone retrieval for reduced spectral resolution (RR) period of MIPAS instrument (2005-2012). Spectroscopy is still the leading error source. The error in vmr at heights below 15 km remains below 0.1 ppmv.

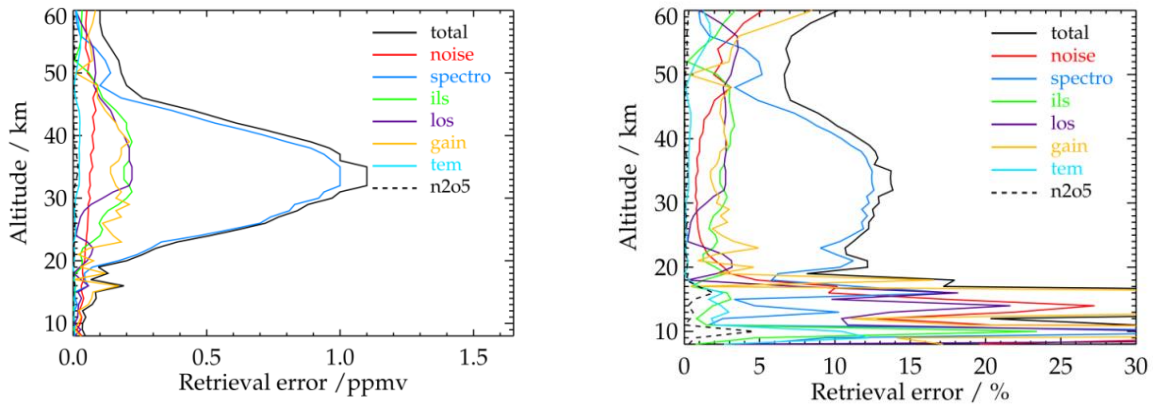

Figure 9: Estimated ozone error budget of MIPAS for a typical RR mid-latitude retrieval (night and day). Left: absolute, right: percentage errors.

4.1.3.2.SCIAMACHY IUP Sciatran

Total systematic ($\pm\sigma_{sys}$) and random ($\pm\sigma_{rnd}$) errors for retrievals of ozone profiles with SCIATRAN processor are calculated, for the three latitude bands and different altitudes in (Rahpoe et al. 2013) and shown as profiles in Figure 10. The contribution to total systematic error is coming from the aerosol (up to 15 %), albedo (up to 8 %), tangent height (up to 8 %), temperature (up to 1 %), and pressure (up to 2 %). The maximum random error is in the order of 43 % in the tropics at 10 km.

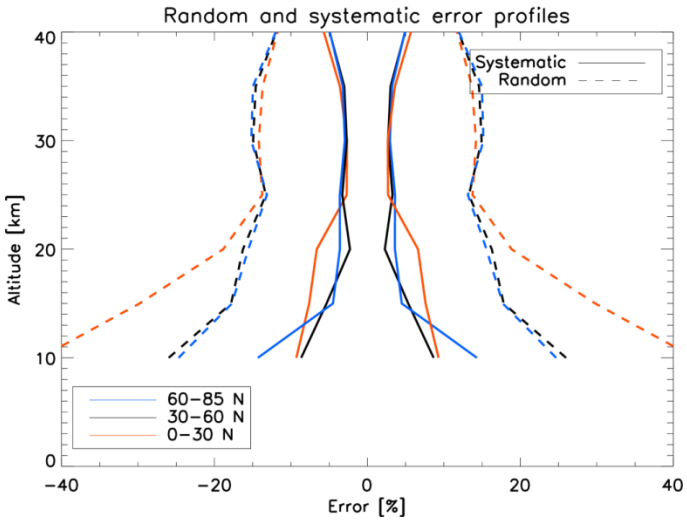

Figure 10: total systematic and random error profiles for three latitude bands for SCIATRAN ozone retrievals.

Lat. Band	Range	10 km	15 km	20 km	25km	30 km	35 km	40 km
Total Systematic								
Tropics	0° – 30° N	9.30	7.61	6.62	2.70	2.67	3.60	5.70
Midlat.	30° – 60° N	8.66	5.34	2.28	3.28	2.70	3.03	4.94
Polar	60° – 85°N	14.32	4.50	3.60	3.61	2.95	3.22	4.91
Total Random								
Tropics	0° – 30° N	42.8	29.8	18.86	13.75	14.20	13.69	11.74
Midlat.	30° – 60° N	25.98	17.82	16.27	13.28	14.94	14.60	11.92
Polar	60° – 85°N	24.69	17.71	15.57	13.14	15.18	14.97	11.98

Table 4: root square sum ±σ in [%] for the three different latitude bands in the northern hemisphere separated for total systematic and total random uncertainties of SCIATRAN ozone retrievals.

4.1.3.3. GOMOS ESA IPF v6

The error estimates (square roots of the diagonal elements of the covariance matrix) are provided in the Level 2 files and the part of the covariance matrix (7 off-diagonal elements). The covariance matrix of retrieved profiles uncertainties is obtained via Gaussian error propagation through the GOMOS inversion, see (Tamminen et al. 2010) for details. As indicated above, both noise and the dominating random modelling error are taken into account on GOMOS inversion. Thus, error estimates provided in Level 2 files, represent the total precision estimates. The precision of GOMOS ozone profiles depends on stellar brightness, spectral class and obliquity of occultation. Typical values of ozone precision values based on real GOMOS data are presented in Figure 11 which shows GOMOS precision estimates of ozone for representative cases: bright star (first column), typical star (middle column) and dim star (last column). The dashed lines correspond to oblique occultations (O) and the solid lines

to vertical (in orbital plane, V) occultations. Stellar temperature is indicated with the line color: hot stars (red), medium stars (green) and cool stars (blue). The uncertainty values are from GOMOS data processed with IPF version 6.

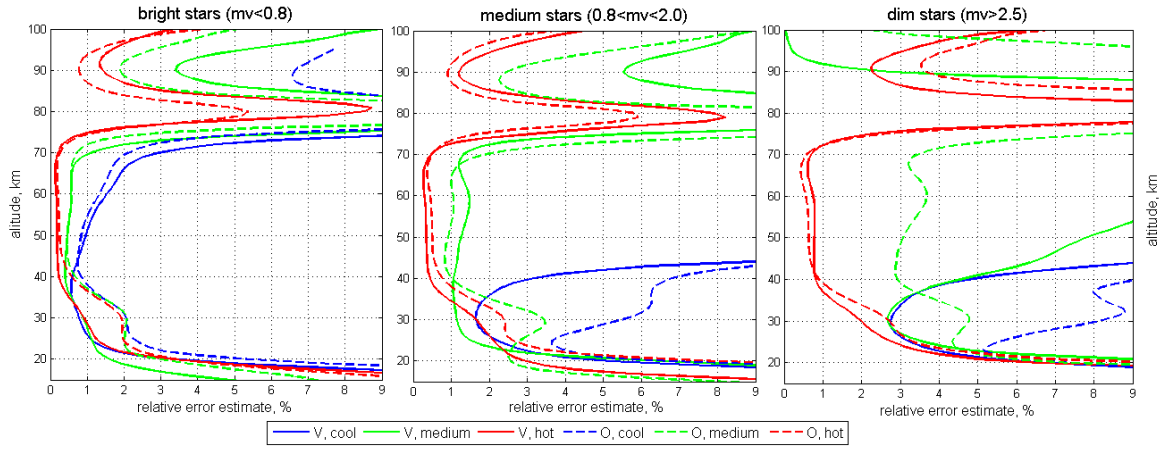

Figure 11: Typical values of ozone precision values based on real GOMOS data.

Other sources of systematic errors are imperfect modelling of the aerosol extinction, uncertainties in the absorption cross sections and temperature. Uncertainties of air density profile, ray tracing and potentially missing constituents have a negligible impact on ozone retrievals. The characteristics of GOMOS ozone profiles together with the random and the systematic errors are summarized in Table 5.

Altitude range	15-100 km
Vertical resolution	2 km below 30 km, 3 km above 40 km
Random errors: measurement noise and scintillations	0.4-4% stratosphere, 2-10 % MLT, ~10% at 15 km
Systematic errors: Uncertainty in cross-sections Aerosol model selection Temperature uncertainty Air density uncertainty	 ~1 % ~20% below 20 km, 1-5% at 20-25 km, <1% above 25 km <0.5% at 30-60 km, negligible elsewhere <1% below 20 km, negligible elsewhere

Table 5: GOMOS ozone profiles characteristics and error budget.

4.1.3.4. OSIRIS/ODIN 5.01

To estimate the OSIRIS ozone error budget a random sampling of scans were chosen and the ozone was repeatedly retrieved with randomly perturbed inputs. The inputs were adjusted by a random factor chosen from a normal distribution of values with a 3σ of 10%. This was performed in turn for the aerosol profile, albedo, neutral density profile, and NO_2 profile. For the altitude registration a 3σ of 300m was used. The precision was calculated using a method described in (Bourassa et al, 2012). The total error shown in the figure above is calculated using a sum in quadrature of the error components.

Figure 12 illustrates the dominance of the precision over the total error budget, which peaks around 7% at approximately 15 km. This is followed by contributions from potential errors in altitude registration, which provides about 2% uncertainty above 35km and below 20km. Errors in the neutral density potentially contribute up to 2% uncertainty at the lowest bounds

of the retrieval and are negligible above 30km. Errors from the other sources are much less than 1% at all altitudes.

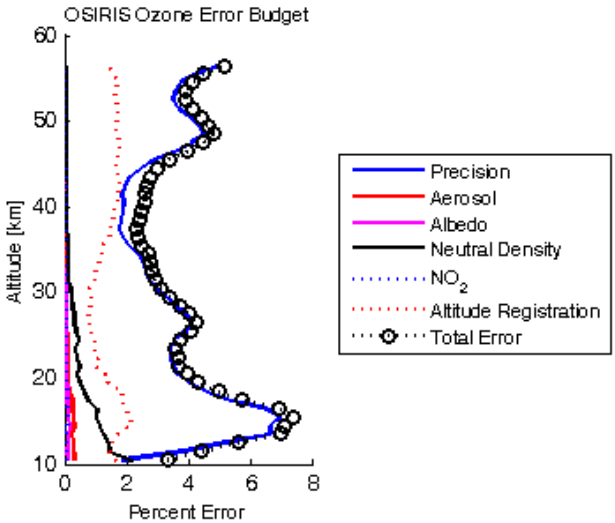

Figure 12: Dominance of the precision over the total error budget of OSIRIS.

4.1.3.5. SMR/ODIN

An advanced analysis of systematic uncertainties of ozone retrieval from ODIN/SMR 501.8 GHz band was performed in (Urban et al. 2005). The ozone retrieval in the 501.8-GHz band is dominated by the spectroscopic model error. The total systematic error is lower than 0.4 ppmv above 25 km and increases to ~0.75 ppmv at 20 km. In terms of relative units, the error is of the order of 5% above 30 km and increases below up to 35% at 20 km. Figure 13 shows instrumental, spectroscopic, and total systematic errors for the ODIN/SMR stratospheric ozone retrieval of the 501.8 GHz band; it includes retrieval error due to uncertainties of collisional line broadening parameters in air, temperature (taken from ECMWF) dependency uncertainty of collisional broadening and uncertainty of spectral line intensities.
Typical altitude resolution of ODIN/SMR ozone product is ~3 km in lower stratosphere, degrading with increasing altitude.

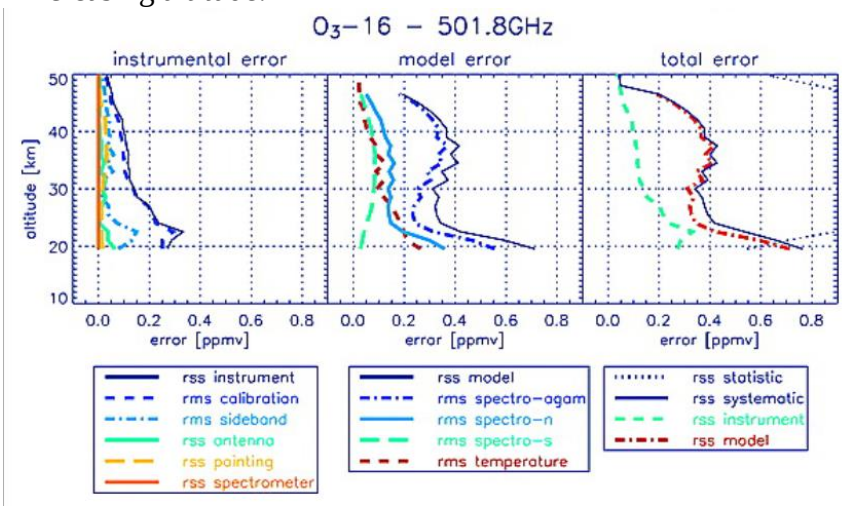

Figure 13: (left) Instrumental, (middle) spectroscopic, and (right) total systematic errors for the ODIN/SMR stratospheric ozone of the 501.8-GHz band.

4.1.3.6. ACE-FTS

Analysis of detailed error budget including systematic errors for the ACE-FTS data products is in progress. Main inputs into the uncertainties are expected to be the strength of the signal and the spectroscopic uncertainties.

The uncertainties reported in the data files are the statistical fitting errors from the least-squares process and do not include systematic components or parameter correlations (Boone et al. 2005). The mean relative fitting errors are lower than 3% between 12 and 62 km and typically less than 2% around the VMR peak (30–35 km), see .

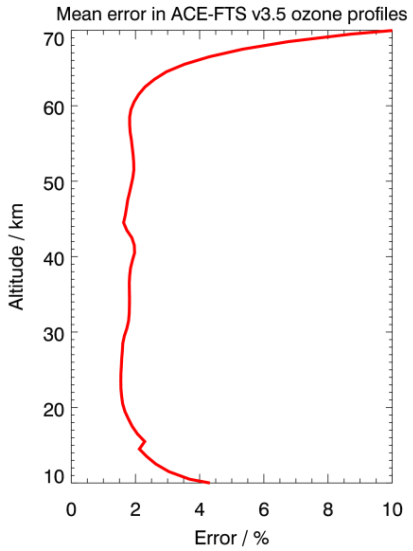

Figure 14: mean uncertainties reported in ACE-FTS v3.5 ozone vertical profiles.

Distribution of the globe of absolute uncertainties reported with ACE-FTS ozone vertical profiles is shown on . The absolute uncertainties values are higher in tropical region, while relative uncertainties are higher in polar regions.

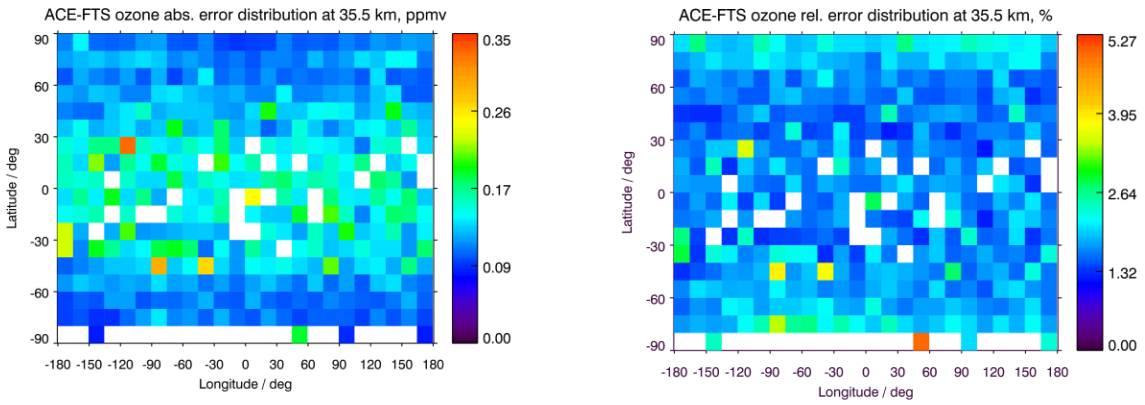

Figure 15: distribution of uncertainties of ozone products from ACE-FTS on 35.5 km height.

Evolution of ACE-FTS ozone uncertainties with time are shown on . One can see that the uncertainties are slightly growing with time, going from 1.7% in the beginning of the mission to 2.0% in the recent period.

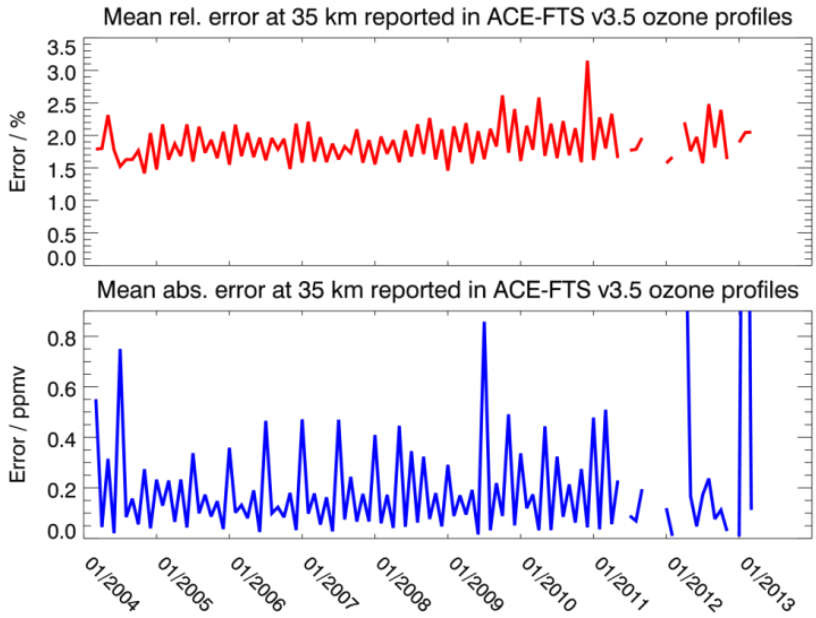

Figure 16: evolution with time of uncertainties of ACE-FTS ozone vertical profiles at 35 km height. Top panel : relative uncertainty, bottom panel: absolute uncertainty.

4.1.3.7. OMPS-LP USask 2D

The OMPS-LP USask 2D retrieval process uses Gaussian error propagation to estimate the covariance of the retrieved solution. Currently only the random error component of the radiance measurements is accounted for. The reported precision is the square root of the diagonal elements of the converged solution covariance matrix. Smoothing error is not included in the reported error estimate, however representative averaging kernels are available as diagnostic quantities.

Error! Reference source not found. shows the output precision estimate for retrieved orbit 12218. The error is largest at low altitudes, reaching values of over 20% just above the tropopause. Throughout most of the middle stratosphere the error estimates are in the range of 4-6%. The observed discontinuities in the stratosphere (e.g. the increase near 30 km) are caused by the phasing out of different wavelengths in the retrieval. The precision estimate does not vary by significant amounts from orbit to orbit, and this orbit is representative of the overall latitudinal structure of the precision.

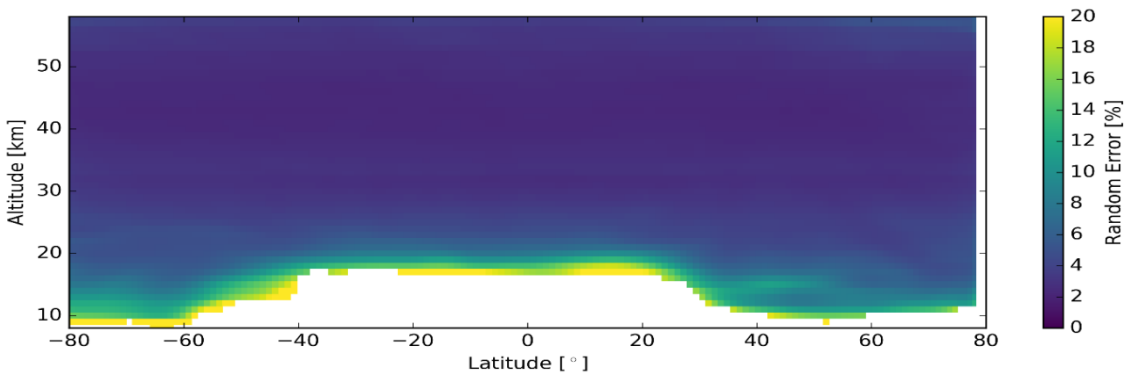

Figure 17: Reported precision estimate for OMPS-LP USask 2D retrieved orbit 12218.

4.2. Validation of precision estimates

Validation of precision estimates (viz., the random component of the estimated uncertainty) is needed when the measurement uncertainty cannot be fully characterized or is based on assumptions. This is especially important for remote-sensing measurements, which use retrievals of atmospheric parameters by solving inverse problems. Precision of the remote sensing measurements is usually estimated via propagation of instrumental noise through the inversion algorithm. These precision estimates can be imperfect due to incomplete forward models or retrieval approximations.

Below we discuss several approaches to validation of precision estimates and their application to Ozone_cci instruments. An overview of the precision validation methods for atmospheric measurements can be also found in (Sofieva et al. 2014).

4.2.1. Approaches to validation of precision estimates and their application to limb vertical profiles

In the laboratory, the experimental precision estimates can be obtained using repeated measurements under the same conditions: the sample variance $s^2 = \mathrm{var}(x)$ approaches the variance of random error distribution σ^2 (i.e., squared precision) when the size of sample N tends to infinity. The sample variance has a χ^2 distribution with $N-1$ degrees of freedom. It can be approximated for large N by a Gaussian distribution with variance

$$\mathrm{var}(s^2) \approx \sigma^4 \frac{2}{N}, \qquad (1)$$

giving the uncertainty of the experimentally estimated precision.

Contrary to laboratory experiments, geophysical observation conditions cannot be kept exactly constant for atmospheric measurements. Therefore, the sample variance contains a contribution due to the natural variability σ_{nat}^2: $s^2 = \sigma^2 + \sigma_{nat}^2$. For validation of uncertainty estimates, σ_{nat}^2 should be minimized by selecting collocated measurements or it should be known from independent sources.

The simplest test, which can confirm that the precision estimates are not overestimated, is comparison of the sample variance s^2 with uncertainty estimates σ^2, s^2 should be always larger than σ^2. Figure 18 shows profiles of s and σ in the tropical stratosphere for Ozone_cci ozone limb profiles. As expected, $s > \sigma$ in GOMOS, MIPAS, OSIRIS and ACE-FTS observations (Figure 18, center). However, the mean uncertainty σ exceeds the sample standard deviation s for SCIAMACHY and SMR in the upper stratosphere. This indicates an overestimation of the random uncertainty component for these instruments. For SCIAMACHY, uncertainty estimate include also a smoothing error; the uncertainty estimates will be revised for the next SCIAMACHY processing version.

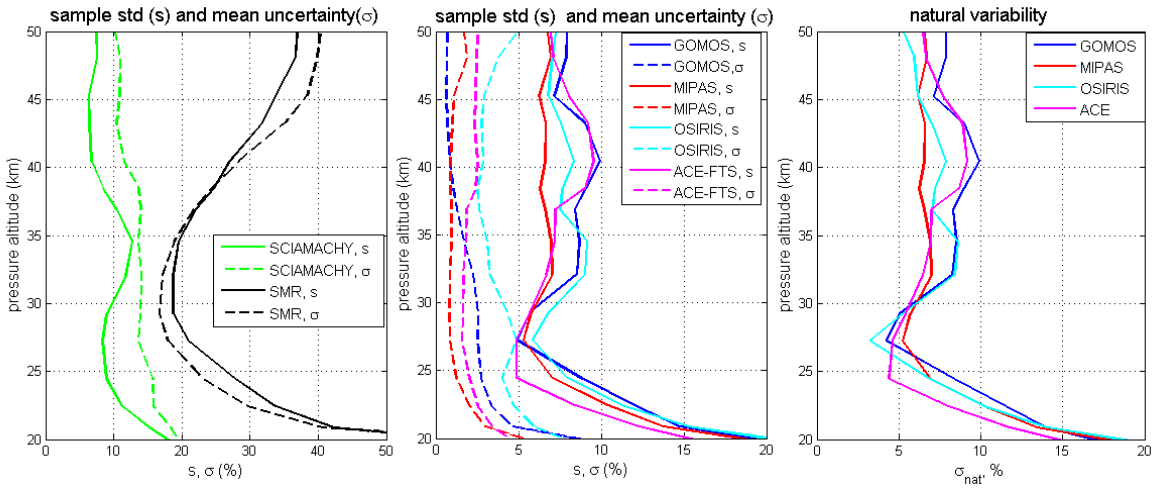

Figure 18 Sample standard deviation s and the mean uncertainty estimates σ in the tropical stratosphere (20S-20N) in 2008, left: SCIAMACHY and SMR, center: GOMOS, MIPAS, OSIRIS and ACE-FTS. Right: the estimates of the natural variability $\sigma_{nat} = \sqrt{s^2 - \sigma^2}$ in the tropics from GOMOS, MIPAS, OSIRIS ad SCIAMACHY.

Approaches to validation of error estimates usually rely on the variance of the difference s_{diff}^2 in a set of collocated measurements x_1 and x_2:

$$s_{diff}^2 = \left\langle \left(x_1 - x_2\right)^2 \right\rangle - \left\langle x_1 - x_2 \right\rangle^2 = \sigma_{0,nat}^2 + \sigma_1^2 + \sigma_2^2 . \qquad (2)$$

In , $\sigma_{0,nat}^2$ stands for the natural variability within a space-time collocation window (note that $\sigma_{0,nat}^2$ is different from σ_{nat}^2), and the angular brackets denote the mean.

Three methods for precision validation have been developed and applied to Ozone_cci measurements.

4.2.1.1. Method 1: using very close self-collocations

For perfectly collocated measurements ($\sigma_{0,nat}^2 \approx 0$) from the same instrument with the same precisions $\sigma_1 = \sigma_2 = \sigma$, Eq. is reduced to $s_{diff}^2 \approx 2\sigma^2$, thus allowing validation of the uncertainty estimate σ. This method was realized, for example, for closely collocated MIPAS and OSIRIS measurements (Piccolo & Dudhia 2007; Bourassa et al. 2012). These studies have concluded that the precision estimates are close to reality.

4.2.1.2. Method 2: evaluation of structure functions

Provided many collocated measurements from the same instrument are available (self-collocations), the precision of the dataset can be estimated also by computing a two- or one-dimensional structure function, or the rms difference as a function of increasing separation in time and in space. Then the limit at zero spatio-temporal mismatch will define the measurement precision.

The parameter $s_{diff}(r)/\sqrt{2}$ approximates the experimental error estimates, which should converge to predicted error estimates when $r \to 0$ (if the latter ones are correct). It is analogous to the integral of structure function, which is widely used in the theory of random

functions (e.g., Yaglom, 1987). In analyses related to the ozone profile measurements by Ozone_cci limb instruments (e.g., Sofieva et al. 2014; Laeng et al. 2015)(Laeng et al. 2013)(Laeng et al. 2013)(Laeng et al. 2013)(Laeng et al. 2013)(Laeng et al. 2013)(Laeng et al. 2013)(Laeng et al. 2013)(Laeng et al. 2013)(Laeng et al. 2013)(Laeng et al. 2013)(Laeng et al. 2013)(Laeng et al. 2013), the distance r represent the separation of air parcels corresponding to collocated measurements with the advection of air masses taken into account.

Since it is practically impossible to find a sufficient number of collocations with very small spatio-temporal separation, it is preferable to evaluate the structure function in the regions of small natural ozone variability. For the limb profile instruments participating in the Ozone_cci project, these are polar regions in local summer. Figure 19 -Figure 21 show the structure functions for MIPAS, OSIRIS and SCIAMACHY. For MIPAS and OSIRIS, the experimental precision estimates $s_{diff}(r)/\sqrt{2}$ decrease with decreasing r and approach rather close the theoretical precision estimates. This confirms the realisticness of precision estimates for these instruments observed also in (Piccolo & Dudhia 2007; Bourassa et al. 2012). The opposite behaviour is for SCIAMACHY: the experimental precision estimates $s_{diff}(r)/\sqrt{2}$ are lower than the theoretical ones. This feature has been already discussed above, it is related to inclusion of the smoothing error in the error budget.

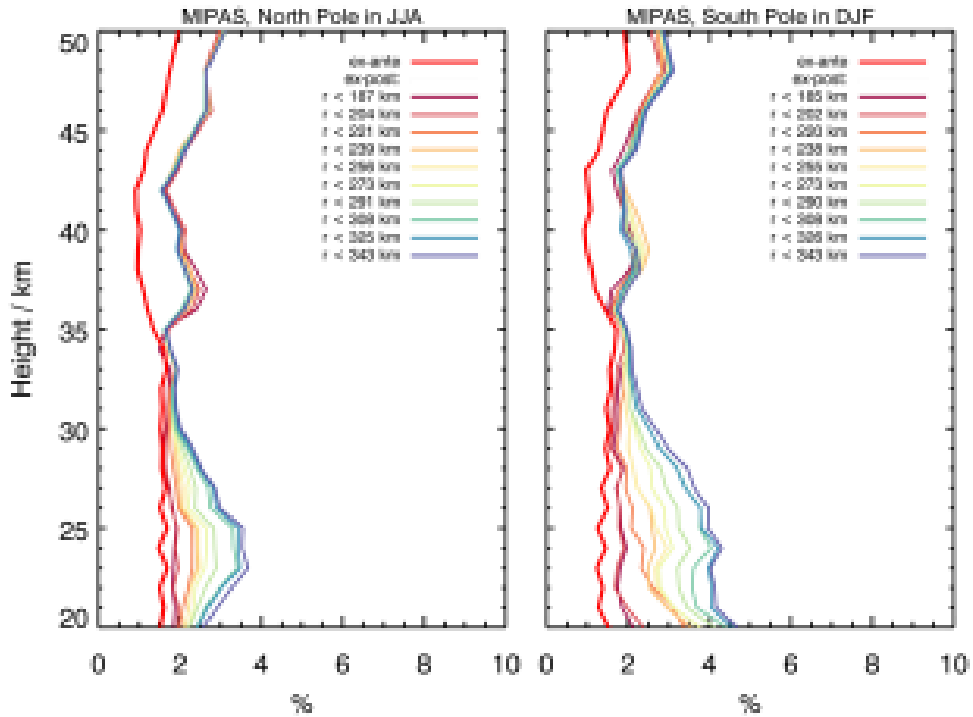

Figure 19: Color lines: experimental precision estimates for different separation distances; black line : mean error estimate.

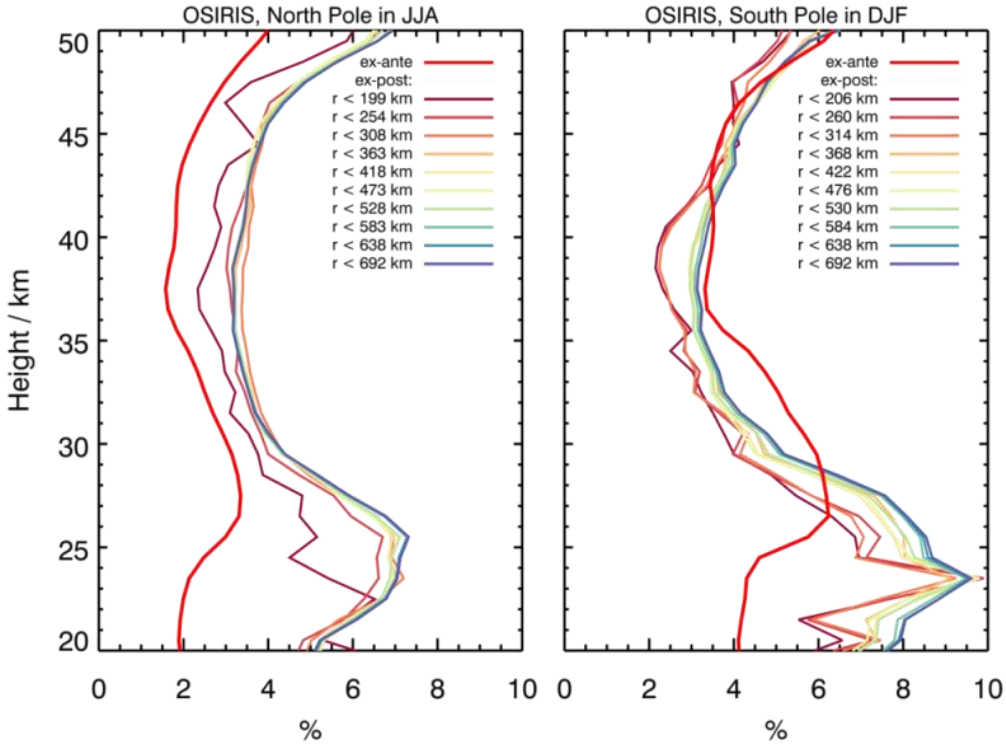

Figure 20: As Figure 19, but for OSIRIS vertical profiles

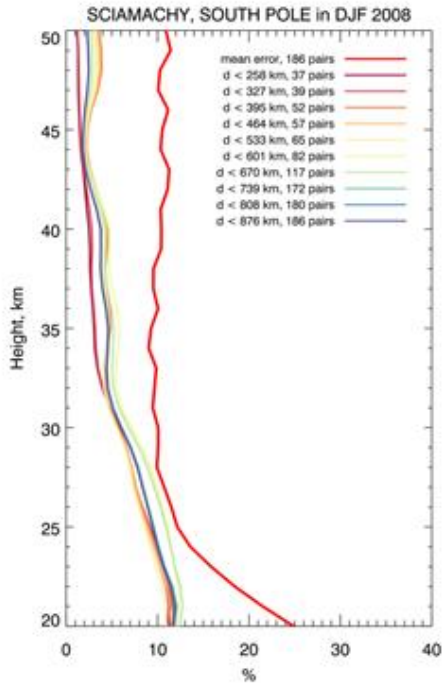

Figure 21: As Figure 19, but for SCIAMACHY ozone vertical profiles close to South Pole in local summer

4.2.1.3. Method 3: differential method

For GOMOS ozone vertical profiles dataset, (Sofieva, 2014) proposed a method for validation of uncertainties by comparing differences of sample variances and squared precision estimates for pairs of stars. The validation of GOMOS precision estimates is especially challenging due to the dependence of the signal-to-noise ratio (and thus precision estimates) on stellar properties and small number of self-collocated measurements. In addition, GOMOS estimated

ozone uncertainties are small in the stratosphere for bright star occultations, which complicates validation of precision values, given the natural ozone variability.
The method is very simple. If the measurements are selected in a region of small and slowly-changing natural variability, then the sample variances corresponding to different datasets *i* (for GOMOS, corresponding to different stars) can be written as $s_i^2 = \sigma_{nat}^2 + \sigma_i^2$. If the precision estimates are correct, then the difference in sample variance will be equal to the difference in precision estimates, $s_i^2 - s_j^2 = \sigma_i^2 - \sigma_j^2$. The term σ_{nat}^2 cancels out because it is assumed to be the same for both samples.
Note that for differential method to work, natural variability should be the same for the samples *i* and *j*; natural variability should not be large compared to the precision estimates, otherwise the sample variance estimates will have large uncertainty, and measurements in each sample should be of the same precision.
The application of the differential method to GOMOS measurements is discussed in detail in (Sofieva et al. 2014). In this work, the samples correspond to occultations of different stars. The authors have found that the GOMOS precision estimates are realistic in occultations of sufficiently bright stars. For dim stars, errors are overestimated due to improper accounting of the dark charge correction uncertainty in the error budget (Sofieva et al. 2014).
The differential method can also be applied to stratospheric ozone data from other instruments, including multi-instrument analyses, as discussed in (Sofieva et al. 2014). In particular, Figure 18 (right) shows the estimates of natural variability $\sigma_{nat} = \sqrt{s^2 - \sigma^2}$ in the tropics for GOMOS, MIPAS, OSIRIS and ACE-FTS. For GOMOS, occultations of stars brighter than magnitude 1.6 are used in the estimates. The profiles of σ_{nat} are close to each other. This proximity also indicated that the precision estimates are close to reality for these instruments. .

4.2.2. Validation of precision estimates of nadir vertical profiles

4.2.2.1. RAL/GOME-2

tbd

4.2.2.2. FORLI/IASI

tbd

4.2.3. Validation of precision estimates of total column datasets

4.2.3.1. GODFIT/GOME-2 and OMI

tbd

4.2.3.2. Observing System Simulation Experiment

Methods based on self-colocations allow us to quantify the uncertainty due to random errors in the satellite data set. However, this technique is blind to any potential systematic error and therefore cannot be used to assess the full measurement uncertainty. For this reason, validation with independent reference measurements remains crucial. However, as illustrated by Eq. (2), the differences between satellite and reference measurements cannot be confronted directly with the reported measurement uncertainties: For all reasonable co-location criteria,

i.e. those resulting in a sufficiently large number of comparison pairs, one must also take into account the additional differences due to co-location mismatch, i.e. differences in spatio-temporal sampling and smoothing of the variable and inhomogeneous ozone field.

A possible approach to quantify these additional uncertainty terms, e.g. $\sigma^2_{0,\mathrm{var}}$ in Eq. (2) when looking at the spread on the differences, is by performing an Observing System Simulation Experiment (OSSE). This method consists in (1) the creation of appropriate observation operators, which quantify the actual 4-D extent of measurement sensitivity of each measurement, (2) application of these observation operators on high-resolution global gridded fields, e.g. from an ozone reanalysis, to simulate the individual measurements, and (3) quantifying the differences between these simulated measurements in an exact copy of the actual validation exercise. When no measurement errors are included in the simulated measurements, this allows an estimate of the differences due solely to co-location mismatch, from which for instance $\sigma^2_{0,\mathrm{var}}$ in Eq. (2) can be derived.

This approach was explored for the validation of O3 CCI total ozone column products by (Verhoelst et al. 2015), and their Figure 12 is reproduced here as Figure 22.

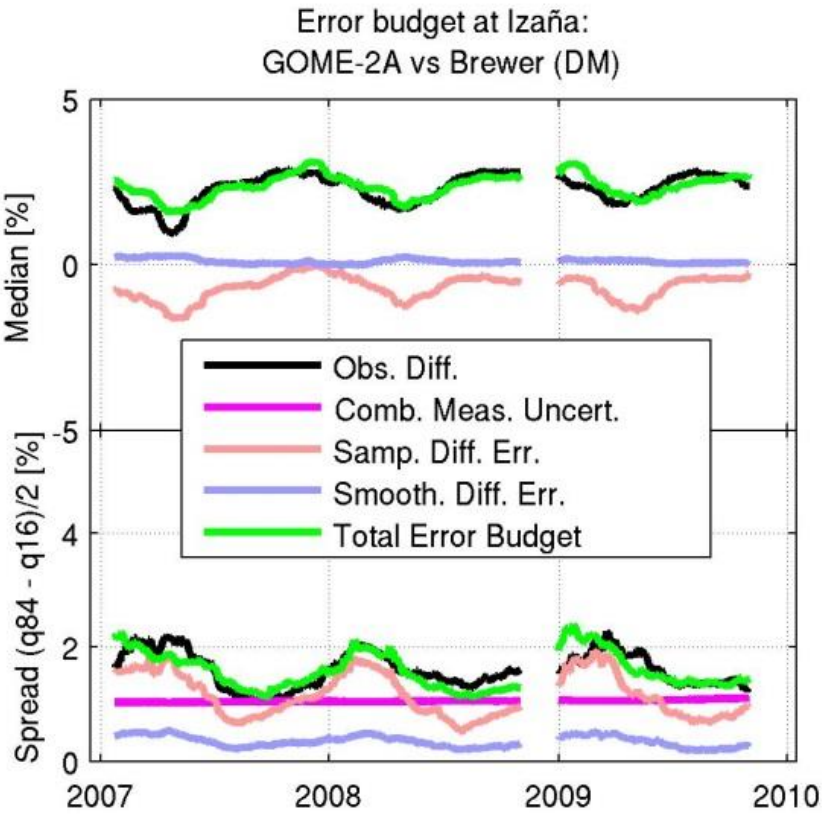

Figure 22: Error budget of comparisons between GODFITv3 GOME-2/MetOp-A total ozone columns and co-located Brewer (daily mean) measurements from the NDACC station at Izana, Canary Islands. The upper panel contains the 3-month median on the differences, the bottom panel the spread (as an interpercentile). Black lines show the statistics of the observed differences, the coloured lines the different components of the OSSE. While the combined measurement uncertainty (magenta) does not account for the observed comparison spread, the error budget can be closed by including the errors due to co-location mismatch. Note that the large median error of approx. 3% is due to the station's mountain top location, due to which the Brewer misses part of the column seen by the larger satellite pixel measuring down to sea level.

Figure 23 illustrates that at first sight, the spread on the differences (black line in the bottom panel) is not consistent with combined reported measurement uncertainties (dashed magenta line). However, when taking into account the simulated sampling (orange) and smoothing (blue) differences, the total error budget (green) does agree with the observed spread on the differences. Similarly, the 3-month median on the differences (upper panel), which is used as a proxy of systematic errors (on at least a seasonal time scale), is in excellent agreement with the simulation, suggesting negligible systematic errors in the satellite data set. (Verhoelst, et al. 2015) performed this analysis across the better part of the NDACC network, and concluded that the GODFITv3 GOME-2A measurement uncertainties as estimated by (Lerot et al. 2014) are potentially too conservative: Random measurement uncertainties of 0.7% (equatorial regions) and 1.0% (mid- to high-latitudes) seem to suffice for error budget closure. As such, this research was an illustration of the successful use of an OSSE to estimate the impact of natural variability in a validation exercise, allowing feedback on the reported measurement uncertainties.

4.2.4. Summary of validation of precision estimates of Level 2 Products

Sensor/algorithm	Product	Quality of uncertainties estimates according to present analysis
OMI/GODFIT	Total column	
GOME-2/RAL	Nadir profile	
IASI	Nadir profile	
GOMOS	Limb profile	realistic for bright stars
MIPAS	Limb profile	realistic
SCIAMACHY	Limb profile	overestimated
ACE-FTS	Limb profile	realistic (via non-robust method)
OSIRIS	Limb profile	realistic
SMR	Limb profile	overestimated (via non-robust method)

Table 6: summary of quality of uncertainties estiates of Level 2 ozone products of Ozone_cci.

5. Uncertainties of Level 3 and Level 4 data

Level 3 data are created using different spatio-temporal averaging. The associated uncertainties are usually estimated as a standard error of the mean:

$$\sigma_{mean}^2 = \frac{s^2}{N}, \qquad (3)$$

where $s^2 = \left\langle (x_k - \bar{x})^2 \right\rangle$ is the sample variance and N is the number of measurements in a spatio-temporal bin. In addition, parameters characterizing spatio-temporal inhomogeneity are provided with the datasets. Below the details of Level 3 uncertainties are presented.

5.1. Ozone total column Level 3 data

The ESA-CCI total ozone level 3 total column ECV product contains monthly averages on a fixed global grid of 1° x 1° in latitude and longitude. A detailed description of the data record can be found in (Coldewey-Egbers 2015).

The level 3 algorithm comprises two parts: at first the level 2 total ozone measurements, processed with the GODFIT_V3 retrieval algorithm (Lerot, 2014), are mapped onto the fixed grid on a daily basis. Each grid cell contains an average of all level 2 data from the same GMT (Greenwich Mean Time) day, that overlap with the level 3 cell. Cell values are computed as weighted averages in which the fractional area of overlap of the satellite ground pixel with the given grid cell is used as weight. The corresponding standard deviation, average area of overlap, and number of level 2 measurements are also provided. Level 2 data can be mapped onto more than one grid cell, and the gridding algorithm is applied separately to the individual GOME, SCIAMACHY, and GOME-2 measurements. Finally the monthly mean level 3 product is computed using the daily gridded averages.

Besides the monthly mean total ozone column, the corresponding standard deviation, the standard error, and the number of measurements per month are provided. The sample standard deviation characterizes the scatter of the measured data encompassing the natural variability, the measurement error as well as the sampling uncertainty. Figure 23 shows standard deviations in April 1997 for GOME, in April 2005 for SCIAMACHY and in April 2008 for GOME-2.

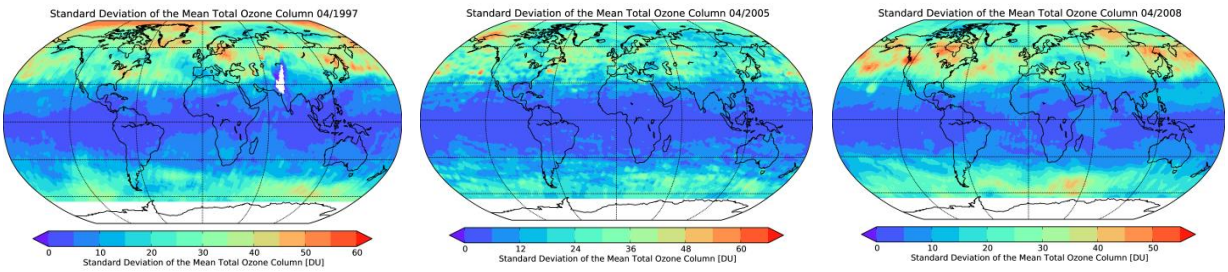

Figure 23: standard deviation of Level 3 ozone total column product in April 1997 for GOME (left panel), in April 2005 for SCIAMACHY (middle panel) and in April 2008 for GOME-2 (right panel).

The standard error quantifies the spatial-temporal sampling errors inherent to the satellite measurements. These errors have been estimated using an Observing System Simulation Experiment (OSSE). Figure 24 shows standard error in April 1997 for GOME, in April 2005 for SCIAMACHY and in April 2008 for GOME-2.

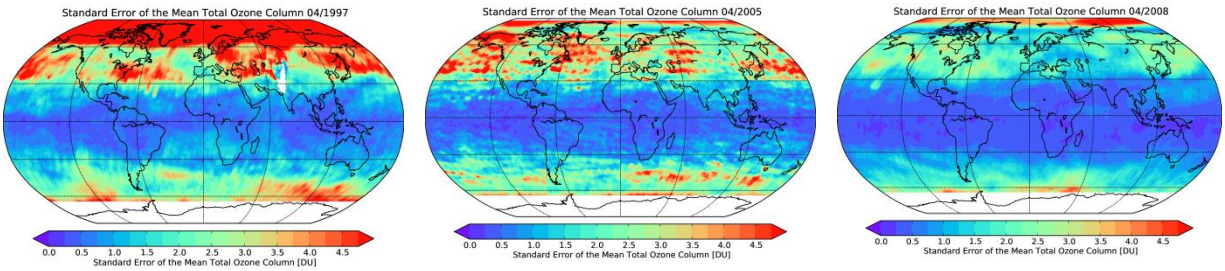

Figure 24: standard error of Level 3 ozone total column product in April 1997 for GOME (left panel), in April 2005 for SCIAMACHY (middle panel) and in April 2008 for GOME-2 (right panel).

High-resolution ECMWF (European Centre for Medium-Range Weather Forecasts, www.ecmwf.eu) data were taken as the reference data set. Then, three sets of daily observations were simulated from the reference using the sampling patterns appropriate to GOME, SCIAMACHY, and GOME-2, respectively. Finally, the average monthly simulations are compared with the corresponding monthly reference in order to estimate the sampling errors corresponding to the total ozone monthly averages.

5.2. Ozone nadir profiles Level 3 data

The pixels in the satellite data (L2) are assumed to be ordered as indicated in Figure 25.

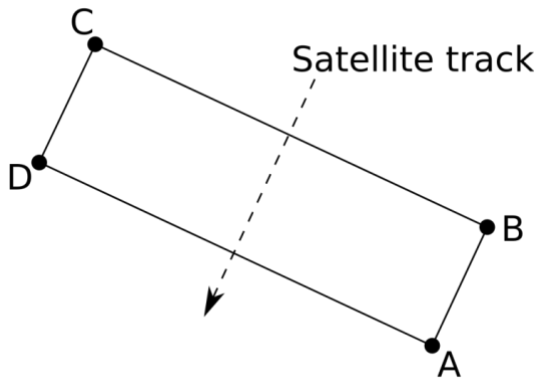

Figure 25: Pixel layout assumed in the nadir L3 algorithm.

If this is not the case, the reading routine should provide the appropriate transformation. **A** is the first corner in the longitude and latitude arrays, **B** the second etc. The across track direction is given by the lines the lines **A**-**D** and **B**-**C**, while the along track direction is given by the lines **A**-**B** and **D**-**C**. Note that corners **C** and **D** are reversed with respect to the GOME/GOME-2 convention.

The along track pixel edges **AB** and **DC** and cross track pixel edges **AD** and **BC** (see Figure 25) are divided into a number of points. The first point on **AB** and the first on **DC** form a line which is divided into into the same number of points as **AD**. Each of these points is assigned to a gridcell, see for example Figure 26.

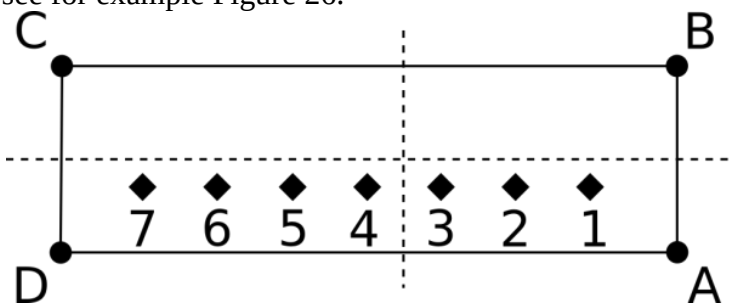

Figure 26: A L2 pixel is divided into subpixels (diamonds 1-7). Each subpixel is assigned to a TM5 gridcell (dashed) and the average and standard deviation are calculated.

Suppose that ABCD in Figure 26 is the pixel of interest and that the horizontal line marked with the diamonds are the subpixels (numbered 1 to 7). Furthermore, the two dashed lines denote the gridcell boundaries which are numbered the same way as the pixel corners (i.e. gridcell A is the lower right cell). In this case, subpixels 1 ~ 3 are added to gridcell A, and the counter for gridcell A is increased by 3. Subpixels 4 ~ 7 are added to gridcell D and the

counter for gridcell D is increased by 4. The pixel values are weighted by $1/\sigma^2$ before adding, so the weighted mean gridcell value and the corresponding standard deviation are given by $mean = \frac{\sum_i \frac{x_i}{\sigma_i^2}}{\sum_i \frac{1}{\sigma_i^2}}$ and $sdev = \sqrt{\frac{1}{\sum_i \frac{1}{\sigma_i^2}}}$. These values are provided for partial columns in the L3 files on a layer-by-layer basis and for the total column. An example is shown in Figure 27 for January 2008, based on the L2 dataset provided in phase 1 of the ozone CCI project.

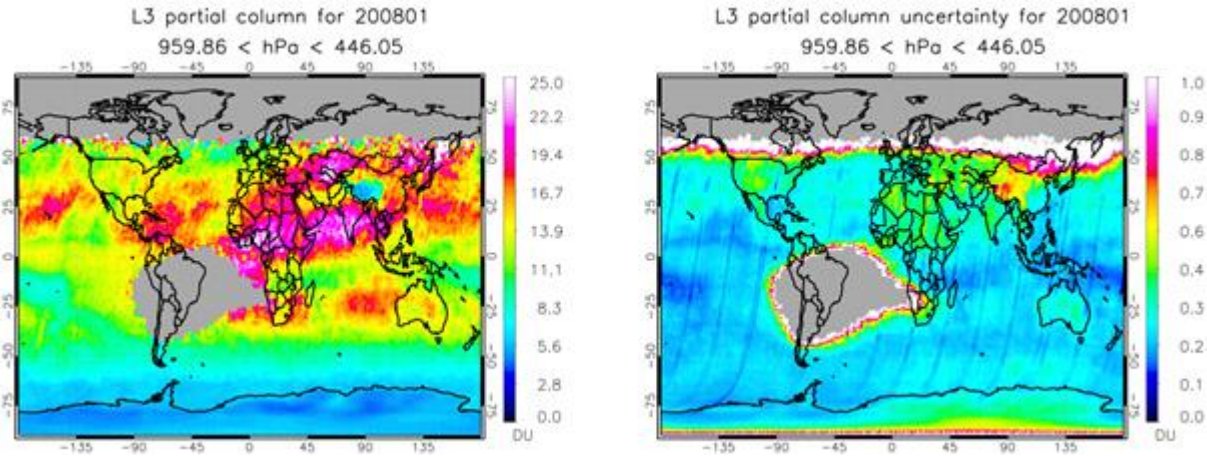

Figure 27: mean partial ozone column (left) and its uncertainty (right) for January 2008, based on L2 data provided in the first phase of the project.

5.3. Ozone nadir profiles Level 4 data

The data assimilation algorithm will take the level-2 data produced by RAL as input. Besides the profiles themselves, other important data that have to be provided in the level-2 product are the averaging kernel (AK) and the covariance matrices. The data are assimilated using the Kalman filter technique that is outlined below. It is basically a form of optimal interpolation to find the weighted average between model results and measurements. Required for this approach are a model and its associated uncertainties (covariance matrix) and the measurements with uncertainties and the averaging kernel. The used model to assimilate the ozone profiles is TM5.

The equations for the statevector $\boldsymbol{x}$ and the measurement vector $\boldsymbol{y}$ are given by:

$$\boldsymbol{x}_{i+1} = M(\boldsymbol{x}_i) + \mathbf{w}_i, \quad \mathbf{w}_i \sim N(\mathbf{0}, \mathbf{Q}_i) \qquad (4)$$

$$\boldsymbol{y}_i = H(\boldsymbol{x}_i) + \mathbf{v}_i, \quad \mathbf{v}_i \sim N(\mathbf{0}, \mathbf{R}_i) \qquad (5)$$

where M is the model that propagates the statevector in time. It has an associated uncertainty $\boldsymbol{w}$, which is assumed to be normally distributed with zero mean and covariance matrix $\mathbf{Q}$. The observation operator H gives the relation between $\boldsymbol{x}$ and $\boldsymbol{y}$. The uncertainty is given by $\boldsymbol{v}$, which is also assumed to have zero mean and covariance matrix $\mathbf{R}$. In matrix notation, the propagation of the statevector and its covariance matrix ($\mathbf{P}$) are given by:

$$\boldsymbol{x}_{i+1} = M(\boldsymbol{x}_i) + \mathbf{w}_i, \quad \mathbf{w}_i \sim N(\mathbf{0}, \mathbf{Q}_i) \qquad (6)$$

$$\boldsymbol{x}_{i+1} = M(\boldsymbol{x}_i) + \mathbf{w}_i, \quad \mathbf{w}_i \sim N(\mathbf{0}, \mathbf{Q}_i) \qquad (7)$$

$$\boldsymbol{x}_{i+1}^f = \mathbf{M}(\boldsymbol{x}_i^a) \qquad (8)$$

$$\mathbf{P}_{i+1}^f = \mathbf{M}\mathbf{P}_i^a\mathbf{M}^T + \mathbf{Q}_i \qquad (9)$$

$\mathbf{P}_{i+1}^f = \mathbf{M}\mathbf{P}_i^a\mathbf{M}^T + \mathbf{Q}_i$where $\boldsymbol{x}^a$ is the statevecctor at time

observations are assimilated according to:

$$\boldsymbol{x}_i^a = \boldsymbol{x}_i^f + \mathbf{K}_i\left(\boldsymbol{y}_i - \mathbf{H}_i\boldsymbol{x}_i^f\right) \quad (10)$$

$$\mathbf{P}_i^a = (\mathbf{I} - \mathbf{K}_i\mathbf{H}_i)\mathbf{P}_i^f \quad (11)$$

$$\mathbf{K}_i = \mathbf{P}_i^f\mathbf{H}_i^T\left(\mathbf{H}_i\mathbf{P}_i^f\mathbf{H}_i^T + \mathbf{R}_i\right)^{-1} \quad (12)$$

where $\mathbf{K}$ is called the Kalman gain matrix.

The covariance matrix $\mathbf{P}$ is too large to handle, it's size is the number of elements in the state vector squared. For TM5 this amounts to $(475200)^2$ elements. To reduce $\mathbf{P}$ to something more manageable we parameterize it into a time dependent standard deviation field and a constant correlation field.

We cannot apply the forecast equation for the covariance matrix directly because of two problems. First, because you have to add $\mathbf{Q}$, the original parameterization is not conserved and $\mathbf{P}$ will "fill up". Eventually, $\mathbf{P}$ will become too large to handle. Second, errors in the ozone chemistry should also be taken into account. Therefore, the Kalman covariance propagation is replaced by an approach where we first apply the model's advection operator to the standard deviation field, and then model the error growth.

In the analysis equations, the number of elements in an ozone profile is generally much larger than the degrees of freedom (about 5 to 6). We therefore reduce the number of datapoints per profile by taking the singular value decomposition of the AK, and transform the profiles accordingly. Finally, we use an eigenvalue decomposition to calculate the $\mathbf{H}_i\mathbf{P}_i^f\mathbf{H}_i^T$ matrix inverse in the Kalman filter equation. We truncate it at a number of eigenvalues representing about 98% of the original trace.

In the L4 files, the ozone concentrations are given as both column densities and volume mixing ratios. The associated uncertainties are given by the time dependent standard deviation field mentioned above. In an example plot is shown for 12 UTC January 31st, 2008, based on the data provided in the first phase of the Ozone-CCI project. The left plot shows the total column, while the right plot shows the uncertainty on the total column, calculated as: $\sigma_{tot} = \sqrt{\sum(\sigma_i)^2}$.

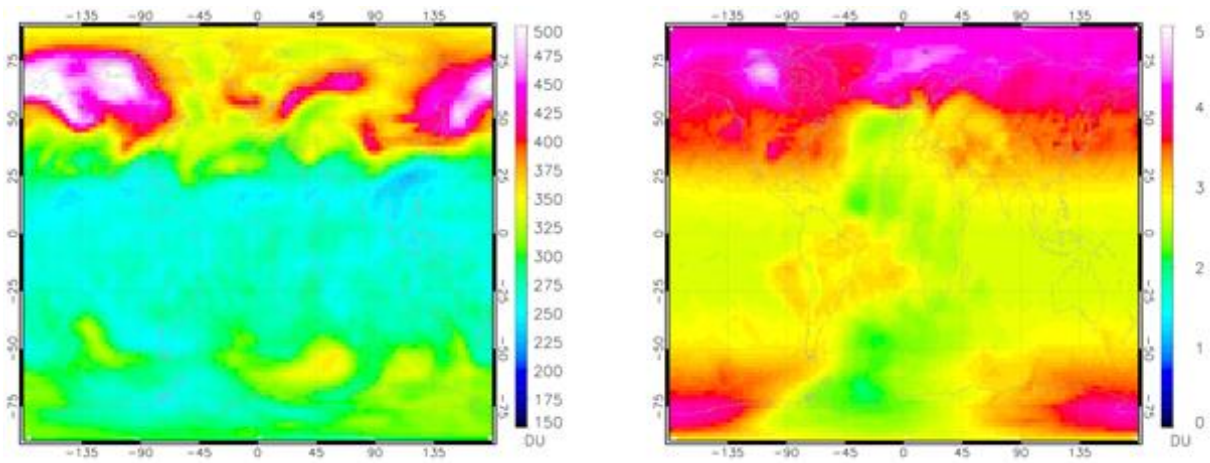

Figure 28: Assimilated total ozone column (left) and the corresponding error for 12 UTC January 31st, 2008, based on L2 data provided in the first phase of the Ozone-CCI project.

5.4. Ozone limb profiles Level 3 data

The uncertainties of Level 3 data from individual instruments (monthly zonal mean and semi-monthly mean profiles) are estimates as the standard error of the mean. The impact of orbital sampling on the standard error of the mean is discussed in details in (Toohey & von Clarmann 2013). Additionally, for characterization patterns, inhomogeneity measures (Sofieva et al., 2014) are provided in the Level 3 data from individual instruments. The inhomogeneity measure is defined as

$$H = \tfrac{1}{2}(A + (1 - E)), \tag{13}$$

where A and E are anisotropy and entropy, respectively (Sofieva et al., 2014). For monthly zonal mean data, inhomogeneity measures in latitude and in time are provided, while for semi-monthly mean profiles also inhomogeneity in longitude is provided. It has been shown (Sofieva et al., 2014) that the inhomogeneity measure can be very useful in characterization of sampling uncertainty. For example, sampling uncertainty of the zonal mean data allows a very simply approximation:

$$\sigma_{sampling} = \frac{1}{2}\left(H_{lat} + H_{time}\right) \cdot \sigma_{nat}, \tag{14}$$

where H_{lat} and H_{time} are inhomogeneity measures in latitude and in time, respectively, and σ_{nat} is a profile of natural variability in the corresponding latitude zone. In Eq.(14), σ_{nat} can be taken from climatology. The total uncertainty of the Level 3 data can be estimates as

$$\sigma^2 = \sigma_{mean}^2 + \sigma_{sampling}^2 \tag{15}$$

Uncertainty of the mean values σ_{mean}, sampling error $\sigma_{sampling}$ and total error σ (Eq.15) of the instrument-based zonal mean data in January 2008 are shown in Figure 29. The standard error of the monthly zonal mean data is well below 1 % in the stratosphere for most of instruments. The sampling uncertainty is small for MIPAS and SCIAMACHY, but it can be as large as a few percent for instruments with a coarser sampling (Figure 29).

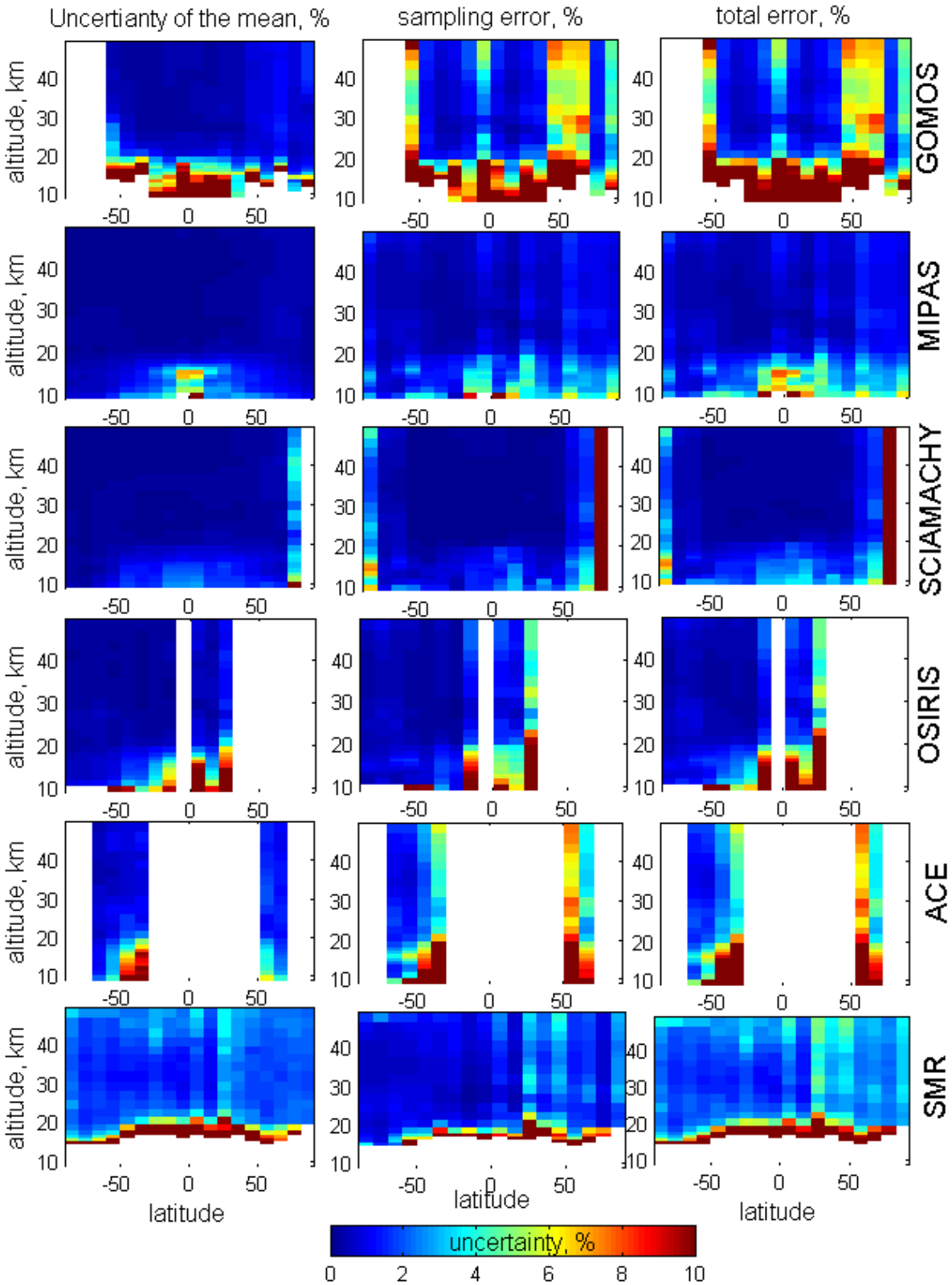

Figure 29: uncertainty of the mean values, sampling error and total error of the instrument-based zonal mean data in January 2008. All uncertainties are presented in %.

In phase 1, the experimental merged Level 3 profiles are computed as the weighted mean of the zonal mean datasets from individual instruments, with the weights α_i that are inversely proportional to total uncertainties σ_i^2 (Eq.16):

$$\rho_{merged} = \sum_{i=1}^{N_{instru}} \alpha_i \rho_i \qquad \alpha_i = \frac{1/\sigma_i^2}{\sum 1/\sigma_i^2} \tag{16}$$

Such weighting has been proposed for monthly zonal mean and semi-monthly mean. The associated uncertainty of the merged dataset will be defined by:

$$\sigma_{merged}^2 = \frac{1}{\sum_{i=1}^{N_{instru}} 1/\sigma_i^2} \cdot \frac{1}{(N_{insru}-1)} \sum_{i=1}^{N_{instru}} \frac{(\rho_i - \rho_{merged})^2}{\sigma_i^2} . \tag{17}$$

The first factor in Eq. 17 , $\frac{1}{\sum_{i=1}^{N_{instru}} 1/\sigma_i^2} = \sigma_{wmean}^2$, is the uncertainty of the weighted mean provided the uncertainties σ_i are the only source of variations in ozone. The second factor in Eq.17 takes into account variability between the datasets. The uncertainties σ_{wmean} and σ_{merged} are shown in Figure 30. As observed in Figure 30, the variability between the datasets has a dominating contribution into uncertainty σ_{merged} of the merged zonal mean data.

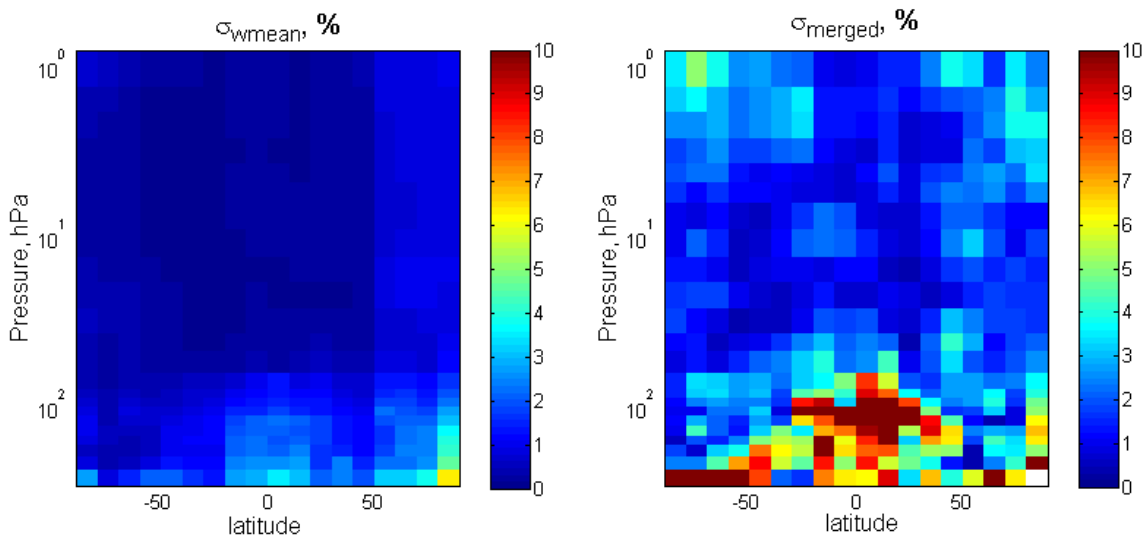

Figure 30: uncertainties associated with the merged monthly mean profile.

For semi-monthly mean data, the typical uncertainties are basically similar to those for monthly zonal mean, but slightly larger (see dedicated TN).

Tropospheric ozone column data

5.5. Tropospheric ozone column data

5.5.1. Limb Nadir Matching (LMN)

The LNM technique is a residual approach that derive tropospheric ozone column (TOC) by subtracting stratospheric O_3 column (SOC), retrieved from the limb observations, from the total O_3 column (TOZ), derived from the nadir observations (Ebojie et al. 2014). The technique requires accurate knowledge of the SOCs, TOZs, tropopause height (TPH), and their associated errors.

The contributions of various error sources to the overall error in the retrieved TOCs are as follows. Clouds are one of the potential error sources, but their effect has been minimized by using TOZ with cloud fractions of less than or equal to 10 % and limb profiles that are not contaminated with clouds. The other potential sources of errors are from the knowledge of SOC, TOZ and the effect of the tropopause height.

The longitudinal structure in errors for three latitude bands 20°N-20°S, 60°N-30°N, and 60°S-30°S are shown in for January 2004 as an example. One can see that among these error sources, the error on SOCs dominates. The errors in TPH are negligible even though highly variable. The errors in TOC are less variable over the globe for the tropical band and highly variable for middle latitudes and presents wave structures.

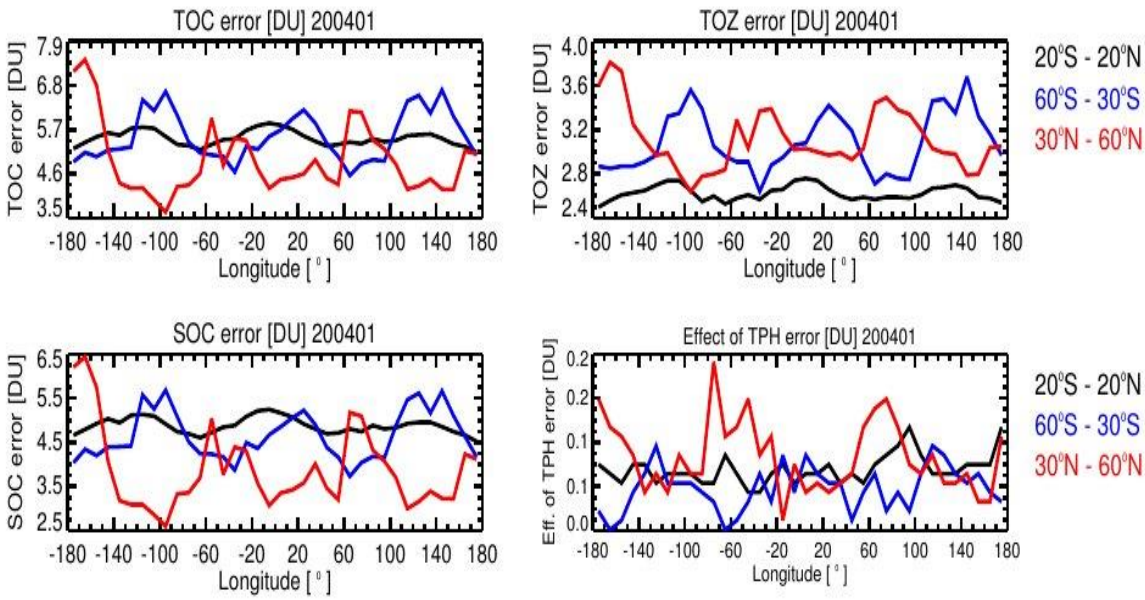

Figure 31: TOZ, SOC and TPH errors' contributions into TOC error.

shows an estimate of the error sources in the TOC retrieval (main input into TOC error) using the SCIAMACHY LNM technique.

Month	Error in temperature ($\sigma = +2$ K)		Error in tangent height ($\sigma = +200$ m)		Error in O_3 cross section (GOME2-SCIAMACHY)		Error in albedo ($\sigma = +0.1$)		Error in aerosol ($\sigma = -40$ %)		Error in pressure ($\sigma = +2$ %)	
	DU	%	DU	%	DU	%	DU	%	DU	%	DU	%
200601	−1.1	−0.4	3.5	1.4	0.2	0.1	−2.0	−0.8	0.0	−0.1	2.3	0.9
200602	−1.2	−0.5	3.5	1.4	0.2	0.1	−2.0	−0.8	0.3	0.0	2.4	0.9
200603	−1.3	−0.5	3.8	1.4	0.2	0.1	−2.1	−0.8	1.0	0.2	2.6	0.9
200604	−1.3	−0.5	3.8	1.4	0.2	0.1	−2.1	−0.8	0.8	0.1	2.6	0.9
200605	−1.2	−0.5	3.6	1.4	0.2	0.1	−2.0	−0.8	0.4	0.1	2.5	0.9
200606	−1.2	−0.5	3.4	1.3	0.2	0.1	−2.0	−0.8	0.4	0.1	2.5	0.9
200607	−1.2	−0.5	3.4	1.3	0.2	0.1	−2.0	−0.8	0.2	0.1	2.4	0.9
200608	−1.2	−0.5	3.4	1.3	0.2	0.1	−2.0	−0.8	0.1	0.1	2.4	0.9
200609	−1.2	−0.5	3.4	1.3	0.2	0.1	−2.0	−0.8	0.2	0.1	2.4	0.9
200610	−1.2	−0.5	3.4	1.3	0.2	0.1	−1.9	−0.8	0.3	0.1	2.4	0.9
200611	−1.2	−0.5	3.4	1.4	0.2	0.1	−1.9	−0.8	0.4	0.1	2.4	0.9
200612	−1.2	−0.5	3.4	1.4	0.2	0.1	−1.9	−0.8	0.6	0.2	2.4	0.9

Table 7: monthly average of global stratospheric ozone column retrieval parameter errors, which is a dominating part of tropospheric ozone column error, in 2006, σ is the assumed parameter uncertainty

5.5.2. Convective Cloud Differential (CCD) Method

The convective cloud differential (CCD) method to retrieve tropospheric ozone columns is applied to level 2 GOME data i.e. ozone vertical columns and cloud data. The stratospheric column is estimated from the above cloud ozone column over high convective clouds. The average of these data over the Indian Ocean, Indonesia to the Pacific is assumed to be representative for the tropics in general. Due to the seasonal migration of the ITCZ latitudinal bands are used. The tropospheric column results from the difference between the total ozone columns for cloud free observations and the above cloud (stratospheric) columns.
There are a few statistical errors in the input data, e.g. from the DOAS fit. The overall error of the total ozone column is stated to be less than 5% of the total column or less than 10 DU. In the gridded data product several tropospheric columns (up to 300) are averaged, so the statistical error should be small. The error in the level 2 input data is also affected by instrument degradation.
There are also some systematic uncertainties in the CCD retrieval:

1. First-order approximation of a zonally invariant stratospheric ozone column in the tropics.

This assumption is justified based on many years of ozone observation from satellites and sondes measurements e.g. in the SHADOZ network. Comparisons of sondes with GOME and GOME-2 measurements (Valks 2003), (Valks et al. 2014) showed small biases (~3DU) for the stratospheric column and rms in the range of 3-7 DU. Hence we can conclude that error introduced by this assumption is less than 10 DU

2. The natural variability of cloud top pressures for high-reflectivity cloud tops lying near the tropopause.

Within one grid cell the standard deviation of the cloud top height is about 2 km at roughly 10 km altitude. The ozone content (4-7 ppb) in this altitude range is estimated in (Valks et al.

2014) using a cloud slicing approach. The maximum error introduced by the different cloud height would be roughly 3 DU. Moreover, we correct for this error in the retrieval, and when averaging several observations the overall error is reduced as long as the difference between the cloud top height (9.2 – 11 km) and the fixed altitude level (10 km) is small.

3. The ozone absorption within the cloud top.

The ozone concentration inside the cloud top can be assumed to be similar to the outside concentration, so we might use the same approximation as for the variability of cloud top pressure. Radiative transfer simulation show that the UV light does not penetrate deep into the cloud, so the error can be estimated to be 1 DU

The main error sources are the variability of the tropospheric columns within a grid cell (~6 to 13 DU) as well as the bias and rmse of the stratospheric column (less than 10 DU), which is of the order of the variation in the stratospheric column within one grid cell. Assuming independence of the three main error sources above, an estimate of total error variance is obtained by summing these three variances. The total error of the tropospheric ozone ccd product is therefore about 10 to 15 DU. The distribution of typical values of CCD tropospheric column uncertainties are shown on . The values on boundaries of retrieval region (20ºS - 20º N) are higher than near the equator.

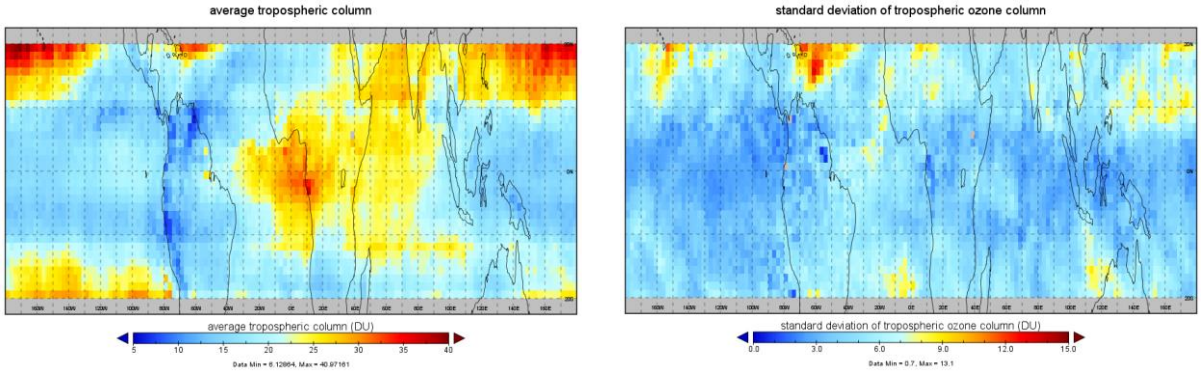

Figure 32: retrieved values (left) and distribution of associated uncertainties (right) for tropospheric ozone column from GOME_2A in March 2013 in [20ºS, 20ºN] band, calculated with CCD method.

The standard deviation of the TCO from the individual observations within a grid cell represents both the atmospheric inhomogeneity and the statistical error of the TCO. Therefore, it is an appropriate estimate of the error.

The standard deviation of the TCO is log-normal distributed with mean values between 3.3 and 4.4 DU, depending on the instrument. The width varies between 1.33 and 1.77 DU. In the merged product the propagated standard deviations of the individual sensors determine the final error to 3.8 ± 1.6 DU.

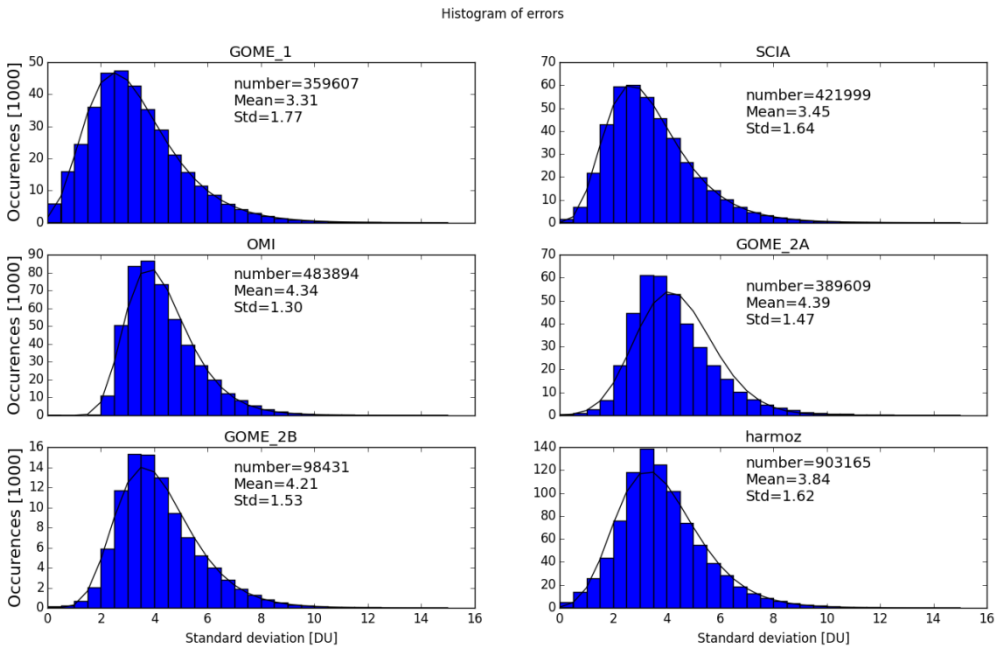

6. References

Boone, C.D. et al., 2005. Retrievals for the atmospheric chemistry experiment Fourier-transform spectrometer. *Appl. Opt.*, 44(33), pp.7218–7231.

Bourassa, A.E. et al., 2012. Precision estimate for Odin-OSIRIS limb scatter retrievals. *J. Geophys. Res.*, 117(D4), p.D04303.

von Clarmann, T., 2014. Smoothing error pitfalls. *Atmospheric Measurement Techniques Discussions*, 7(4), pp.3301–3319. Available at: http://www.atmos-meas-tech-discuss.net/7/3301/2014/.

Coldewey-Egbers, M. et al, 2015. The GOME-type Total Ozone Essential Climate Variable (GTO-ECV) data record from the ESA Climate Change Initiative. *Atmos. Meas. Tech. Discuss.*, 8.

Dufour, G. et al., 2012. Validation of three different scientific ozone products retrieved from IASI spectra using ozonesondes. *Atmospheric Measurement Techniques*, 5(3), pp.611–630.

Dupuy, E. et al., 2008. Validation of ozone measurements from the Atmospheric Chemistry Experiment (ACE). , pp.2513–2656.

Ebojie, F. et al., 2014. Tropospheric column amount of ozone retrieved from SCIAMACHY limb–nadir-matching observations. *Atmospheric Measurement Techniques*, 7(7),

pp.2073–2096.

Hurtmans, D. et al., 2012. FORLI radiative transfer and retrieval code for IASI. *Journal of Quantitative Spectroscopy and Radiative Transfer*, 113(11), pp.1391–1408.

Kerridge, B.J.K. et al., 2002. *GOME-2 Error Assessment Study. Final Report EUMETSAT Contract No EUM/CO/01/901/DK.*,

Laeng, A. et al., 2013. The Ozone Climate Change Initiative: Comparison of four Level 2 Processors for the Michelson Interferometer for Passive Atmospheric Sounding (MIPAS). *Remote Sensing of Environment*, submitted.

Laeng, A. et al., 2015. The ozone climate change initiative: Comparison of four Level-2 processors for the Michelson Interferometer for Passive Atmospheric Sounding (MIPAS). *Remote Sensing of Environment*, 162(0), pp.316–343.

Laeng, A. et al, 2016. Geophysical validation of uncertainty estimates of ozone datasets from Ozone_cci project. *in preparation*.

Lerot, C. et al., 2014. Homogenized total ozone data records from the European sensors GOME/ERS-2, SCIAMACHY/Envisat, and GOME-2/MetOp-A. *Journal of Geophysical Research: Atmospheres*, 119(3), pp.1639–1662.

Miles, G.M. et al., 2015. Tropospheric ozone and ozone profiles retrieved from GOME-2 and their validation. *Atmospheric Measurement Techniques*, 8(1), pp.385–398.

Piccolo, C. & Dudhia, A., 2007. Precision validation of MIPAS-Envisat products. *Atmospheric Chemistry and Physics*, 7(8), pp.1915–1923. Available at: http://www.atmos-chem-phys.net/7/1915/2007/.

Rahpoe, N. et al., 2013. Error budget analysis of SCIAMACHY limb ozone profile retrievals using the SCIATRAN model. *Atmos. Meas. Tech. Discuss.*, 6, pp.4645–4676.

Siddans, R., 2003. *Height Resolved Ozone Retrievals from Global Ozone Monitoring Experiment.* University of Reading, 2003.

Sofieva, V.F. et al., 2014. Validation of GOMOS ozone precision estimates in the stratosphere. *Atmospheric Measurement Techniques*, 7(7), pp.2147–2158. Available at: http://www.atmos-meas-tech.net/7/2147/2014/.

Steck, T. et al., 2007. Bias determination and precision validation of ozone profiles from {MIPAS-Envisat} retrieved with the {IMK-IAA} processor. *Atmos. Chem. Phys. Discuss.*, 7, pp.4427–4480.

Tamminen, J. et al., 2010. GOMOS data characterisation and error estimation. *Atmos. Chem. Phys.*, 10(19), pp.9505–9519.

Toohey, M. & von Clarmann, T., 2013. Climatologies from satellite measurements: the impact of orbital sampling on the standard error of the mean. *Atmospheric Measurement Techniques*, 6(4), pp.937–948. Available at: http://www.atmos-meas-tech.net/6/937/2013/.

Urban, J. et al., 2005. Odin/SMR limb observations of stratospheric trace gases: Level 2 processing of ClO, N_2O, HNO_3, and O_3. *Journal of Geophysical Research: Atmospheres*, 110(D14), p.D14307. Available at: http://dx.doi.org/10.1029/2004JD005741.

Valks, P. et al., 2014. Tropical tropospheric ozone column retrieval for GOME-2. *Atmospheric Measurement Techniques*, 7(8), pp.2513–2530.

Valks, P.J.M. et al, 2003. Variability in tropical tropospheric ozone: Analysis with Global Ozone Monitoring Experiment observations and a global model. *Journal of Geophysical Research*, 108(D11), p.4328.

Verhoelst, T., Granville, J., Hendrick, F., Kohler, U., et al., 2015. Metrology of ground-based satellite validation: Co-location mismatch and smoothing issues of total ozone comparisons. *Atmospheric Measurement Techniques*, 8(12), pp.5039–5062.

Verhoelst, T., Granville, J., Hendrick, F., Köhler, U., et al., 2015. Metrology of ground-based

satellite validation: location mismatch and smoothing issues of total ozone comparison. *Atmos. Meas. Tech. Discuss.*

Wespes, C. et al., 2009. Global distributions of nitric acid from IASI/MetOP measurements. *Atmospheric Chemistry and Physics*, 9(20), pp.7949–7962.

Yaglom, A.M., 1987. *Correlation theory of stationary and related random functions*, Springer Verlag.